69P

1531

DETERMINATION OF BAND OSCILLATOR STRENGTHS OF ATMOSPHERIC MOLECULES FROM HIGH RESOLUTION VACUUM ULTRAVIOLET CROSS SECTION MEASUREMENTS

Grant NAG 5-484

Semiannual Status Report No. 3

For the period 1 November 1985 through 30 April 1986

Principal Investigator
W.H. Parkinson

May 1986

Prepared for
National Aeronautics and Space Administration
Greenbelt, Maryland 20771

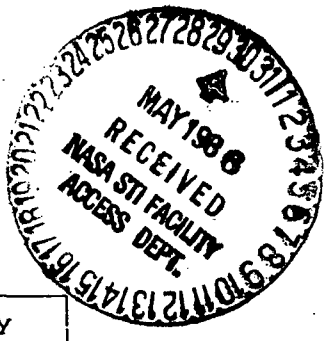

Smithsonian Institution
Astrophysical Observatory
Cambridge, MA 02138

The Smithsonian Astrophysical Observatory
is a member of the
Harvard-Smithsonian Center for Astrophysics

The NASA Technical Officer for this grant is Dr. Igor J. Eberstein, Code 616, Goddard Space Flight Center, Greenbelt, Maryland 20771

Abstract

An account is given of progress during the six month period 11/1/85 - 4/30/86 in work on (a) the determination of band oscillator strengths of the Schumann-Runge absorption bands of $^{16}O_2$ and $^{18}O_2$ from cross section measurements conducted at 79 K; (b) the determination of the absolute absorption cross section of the Schumann-Runge bands of $^{16}O^{18}O$ from optical depth measurements performed on mixtures of $^{16}O_2$, $^{18}O_2$ and $^{16}O^{18}O$ at 79K; and (c) the influence of Schumann-Runge line-wing contributions on the determination of the Herzberg continuum absorption cross section of $^{16}O_2$ in the wavelength region 194-204 nm. The experimental investigations relevant to (a) - (c) are effected at high resolution with a 6.65 m scanning spectrometer which is, by virtue of its small instrumental width (FWHM = 0.0013 nm), uniquely suitable for cross section measurements of molecular bands with discrete rotational structure. Absolute cross sections, which are independent of the instrumental function and from which band oscillator strengths are directly determined, are measured for the absorption bands that are most predissociated. Such measurements are needed for (1) accurate calculations of the stratospheric production of atomic oxygen and heavy ozone formed following the photopredissociation of $^{18}O^{16}O$ by solar radiation penetrating between the absorption lines of $^{16}O_2$; (2) elucidation of the mechanism of predissociation of the upper state of the Schumann-Runge bands; and (3) determination of the true shape of the Herzberg continuum cross section.

PROGRESS REPORT FOR THE PERIOD 11/1/85 - 4/30/86

(a) Schumann-Runge Bands of $^{18}O_2$

In our last semi-annual report, for the period 5/1/85 - 10/31/85, we presented in Fig. 2 of that report absolute absorption cross section measurements of the (14,0), (13,0) and (11,0) through (2,0) Schumann-runge bands of $^{18}O_2$ at 79 K. Of the (2,0) - (14,0) bands, only the (12,0) proved to be so sharp (i.e., so little predissociated) that its absolute cross section cannot be obtained with our instrumental width of 0.0013 nm.

The other twelve band oscillator strengths, f(v',0), have been obtained by direct numerical integration of the measured cross section, $\sigma(\nu)$, over the entire rotational structure of each band:

$$f(v',0) = 1.130 \times 10^{12} \int_{band} \sigma(\nu)\, d\nu$$

The principal advantage of making the cross section measurements at 79 K is that the development of the rotational structure to high rotational quantum numbers is curtailed, with the result that overlapping with the band head region of the (v'-1,0) band does not occur. Consequently, the extrapolations to high N values that are necessary at 300 K become unnecessary at 79 K, with a concomitant increase in the accuracy of the band oscillator strength determination.

In Table 1 we present our results for the band oscillator strengths of the Schumann-Runge bands of $^{16}O_2$ and $^{18}O_2$, as determined from cross sections measured at 79 K. For the (2,0) through (11,0) bands, the ratios of band oscillator strengths of $^{18}O_2$ to those of $^{16}O_2$ increase from 0.308 to 0.545. We believe this effect is largely the result of

the isotopic variation of the Franck-Condon factors. These results will be discussed in more detail after our results for the band oscillator strengths of $^{16}O^{18}O$ become available.

(b) Schumann-Runge Bands of $^{16}O^{18}O$

In our last semi-annual report, we noted that optical depth measurements had been made on mixtures at 79 K of $^{16}O_2$, $^{16}O^{18}O$ and $^{18}O_2$ of nominal composition 25% $^{16}O_2$, 50% $^{16}O^{18}O$ and 25% $^{18}O_2$. The 50 cm long absorption cell was cooled with liquid nitrogen, and photoabsorption measurements were made throughout the region 179-200 nm. Cross sections derived from measured optical depths and the provisional assumption that the column density of each isotope corresponds to the total measured pressure have been obtained. For the (9,0) bands, such results are shown in Fig. 1. To obtain the correctly normalized absolute cross section of $^{16}O^{18}O$, corresponding to its actual concentration in the isotopic mixture, we derive the actual column densities of $^{16}O_2$ and $^{18}O_2$ from their now known cross sections and measured optical depths in the mixture, and we attribute the remaining column density required to account for the total measured column density (pressure) to $^{16}O^{18}O$. The final cross section for the (9,0) band of $^{16}O^{18}O$, obtained after subtraction of the cross sections of $^{16}O_2$ and $^{18}O_2$, is shown in Fig. 2.

Band oscillator strengths of $^{16}O^{18}O$ will be determined by integration of the cross sections, of which the (9,0) cross section in Fig. 2 is an example.

(c) Schumann-Runge Line-Wing Contributions to the Continuum Cross Section of Oxygen in the Region 194-204 nm

In the region 194-204 nm, the measured attenuation of radiation arises from the Herzberg absorption continuum of O_2, a pressure-dependent absorption due to 2 molecules of O_2, absorption due to Schumann-Runge lines, and Rayleigh scattering. The cross section measured at the local minima between Schumann-Runge lines contains, inter alia, significant contributions from the Schumann-Runge line-wings and these contributions mask the true shape of the Herzberg continuum. Allowance for this effect and the derivation of true shape of the Herzberg continuum are dealt with in Sections 3.7, 4 and 5 of the preprint titled "Absorption Cross Section Measurements of Oxygen in the Wavelength Region 195-241 nm of the Herzberg Continuum" by Cheung, Yoshino, Parkinson, Guberman, and Freeman. A copy of this paper, which has been submitted to Planetary and Space Science, is contained in the Appendix.

(d) Publications and Presentations

The following is a cumulative listing of items supported by the NASA grant NAG 5-484:

K. Yoshino, D.E. Freeman, and W.H. Parkinson, "Atlas of the Schumann-Runge Absorption Bands of O_2 in the Wavelength Region 175-205 nm." J. Phys. Chem. Ref. Data, **14**, 207-227 (1984).

K. Yoshino, D.E. Freeman, A.S.-C. Cheung, and W.H. Parkinson, "Schumann-Runge Absorption Bands of $^{18}O_2$." Presented at the Symposium on Molecular Spectroscopy at the Ohio State University in June 1985.

P.L. Smith, H.E. Griesinger, J.H. Black, K. Yoshino, and D.E. Freeman, "Interstellar O_2. II. VUV Oscillator Strengths of Schumann-Runge Lines and Prospects for Space Telescope Observations." Astrophys. J., **277**, 569-575 (1984).

A.S.-C. Cheung, K. Yoshino, W.H. Parkinson, S.L. Guberman, and D.E. Freeman, "Absorption Cross Section Measurements of Oxygen in the Wavelength Region 195-241 nm of the Herzberg Continuum." Submitted in April 1986 to Planet. Space Sci.

TABLE 1. SCHUMANN-RUNGE BAND OSCILLATOR STRENGTHS OF O_2, $f(v',0)$ in 10^{-x}, DETERMINED FROM ABSOLUTE CROSS SECTION MEASUREMENTS AT 79 K

v'	x	$f(v',0;^{16}O_2)$	$f(v',0;^{18}O_2)$	$\frac{f(v',0;^{18}O_2)}{f(v',0;^{16}O_2)}$
2	8	1.90	0.586	0.308
3	8	8.36	2.86	0.342
4	7	2.71	1.01	0.373
5	7	7.39	2.85	0.386
6	6	1.63	0.682	0.418
7	6	3.36	1.51	0.449
8	6	5.92	2.79	0.471
9	6	9.06	4.61	0.509
10	5	1.39	0.747	0.537
11	5	1.91	1.04	0.545
12	5	2.24	-	-
13	5	-	1.66	-
14	5	-	1.90	-

Fig. 1. Cross section measurements of the (9,0) Schumann-Runge bands of isotopic oxygen at 79 K. The ratio of the concentrations of $^{16}O_2$, $^{16}O^{18}O$ and $^{18}O_2$ is approximately 1:2:1. X in the ordinate label σ.X is approximately 0.25 for $^{16}O_2$ and $^{18}O_2$ and 0.50 for $^{16}O^{18}O$.

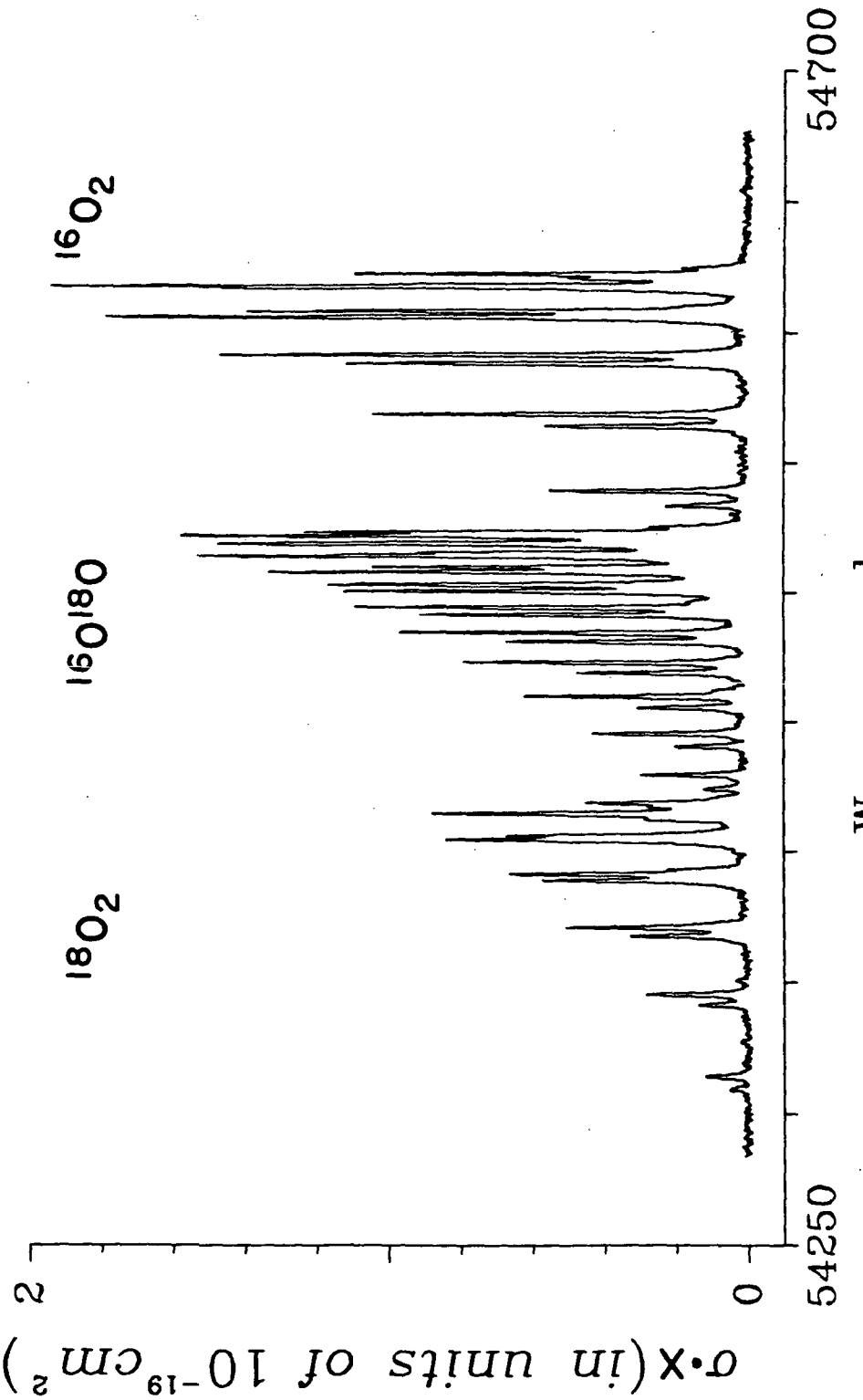
$\sigma \cdot X$ (in units of $10^{-19} cm^2$)
2
0
54250
54700
Wavenumber
$^{18}O_2$
$^{16}O^{18}O$
$^{16}O_2$

Fig. 1

Fig. 2. Absolute absorption cross section measurement of the (9,0) Schumann-Runge band of $^{16}O^{18}O$ obtained from a mixture of $^{16}O_2$, $^{16}O^{18}O$ and $^{18}O_2$ at 79 K.

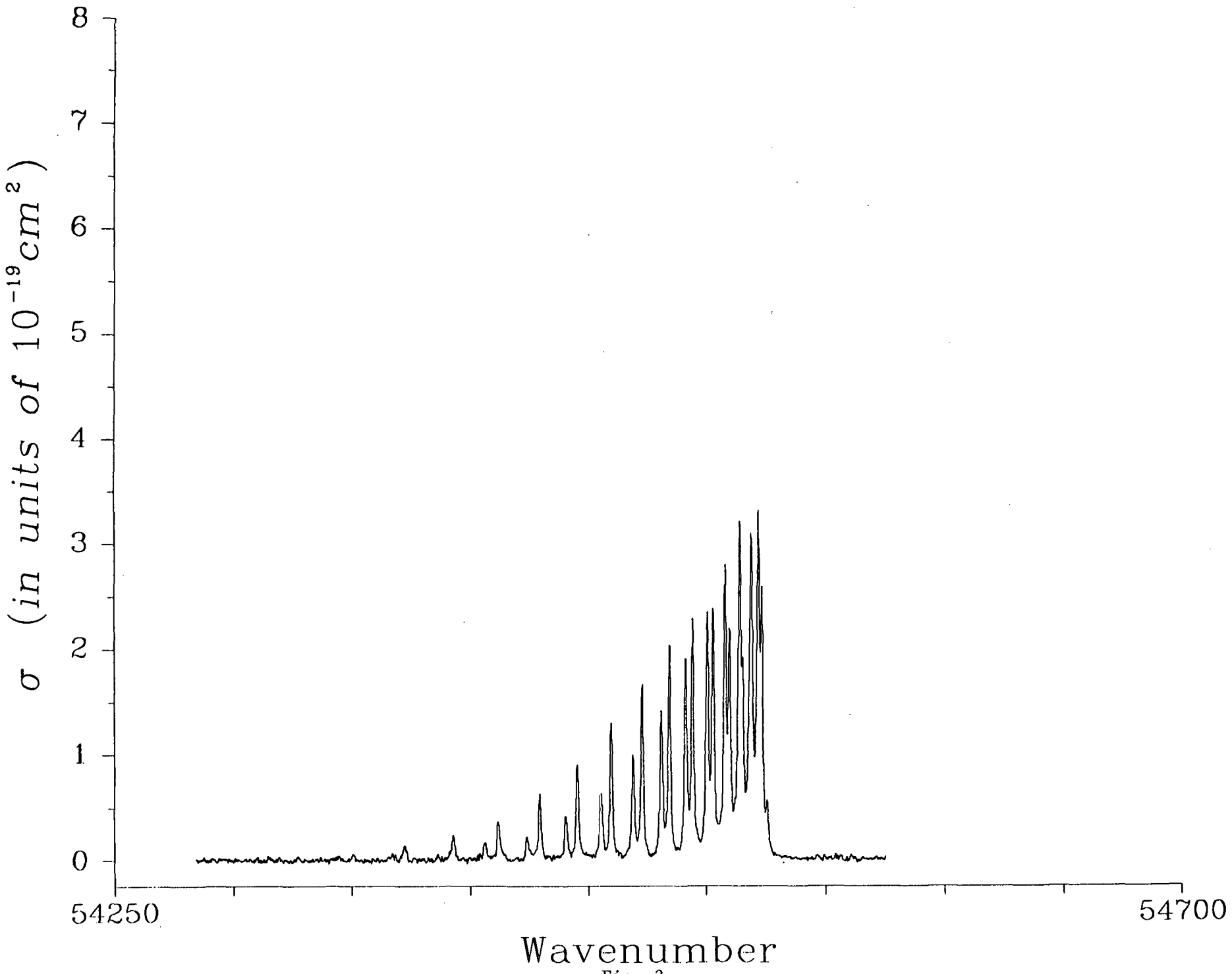

Fig. 2

APPENDIX

ABSORPTION CROSS SECTION MEASUREMENTS OF OXYGEN IN THE WAVELENGTH REGION 195-241 nm OF THE HERZBERG CONTINUUM

A.S.-C. Cheung,*† K. Yoshino,* W.H. Parkinson,*

S.L. Guberman,*‡ and D.E. Freeman*

*Harvard-Smithsonian Center for Astrophysics, Cambridge, MA 02138, U.S.A.

‡Institute for Scientific Research, 271 Main St., Stoneham, MA 02180, U.S.A.

Running Head: Cross section of oxygen in the region 195-241 nm

Proofs to:
Dr. D.E. Freeman
Harvard-Smithsonian Center for Astrophysics
60 Garden Street
Cambridge, MA 02138, U.S.A.

†Present Address: Department of Chemistry, University of Hong Kong, Hong Kong

Abstract

The continuum cross section of oxygen at 296-300 K has been measured with a resolution of 0.13 nm throughout the wavelength region 205-241 nm with oxygen pressures from 5 to 760 torr and optical path lengths from 13.3 to 133 m. The three processes contributing to the observed cross section are absorption into two kinds of continua, viz., the Herzberg continua of O_2 and a pressure-dependent continuum involving two molecules of O_2, and Rayleigh scattering. Extrapolation of the observed cross section to zero pressure yields the continuum cross section of O_2, from which the calculated Rayleigh scattering is subtracted to give the Herzberg continuum absorption cross section of O_2. Our previous continuum cross sections [Cheung et al. (1984) Can. J. Phys. 62, 1752], obtained from studies at high resolution (0.0013 nm) between the Schumann-Runge absorption lines in the region 194-204 nm, are here adjusted for Schumann-Runge line-wing contributions. These adjusted cross sections are compared with those calculated from computed Franck-Condon densities and a transition moment extrapolated from that calculated from our more accurate cross section measurements at longer wavelengths. Our calculated cross section in the region 195-237 nm is similar in shape to that calculated by Saxon and Slanger [J. Geophys. Res., to be published] from the transition moments computed ab initio by Klotz and Peyerimhoff [Mol. Phys., to be published]. Our values of the Herzberg continuum cross section of oxygen, tabulated at 1 nm intervals in the region 195-241 nm, increase from 6.3×10^{-24} cm^2 at 195 nm to a maximum of 6.6×10^{-24} cm^2 at 201 nm and then decrease to 0.85×10^{-24} cm^2 at 241 nm. Our results agree with those in the region 205-225 nm covered by the most recent previous laboratory study [Johnston et al.

(1984) J. Geophys. Res. 89, 11661] and are consistent with values in the region 200-220 nm spanned collectively by three in situ stratospheric studies [Frederick and Mentall (1982) Geophys. Res. Lett. 9, 461; Herman and Mentall (1982) J. Geophys. Res. 87, 8967; Anderson and Hall (1983) J. Geophys. Res. 88, 6801]. The larger Herzberg continuum cross sections found in another in situ stratospheric study [Pirre et al. (1984) Geophys. Res. Lett. 11, 1199] are in definite disagreement with our laboratory values, certainly in the region 205-214 nm. Our Herzberg continuum cross sections in the region 195-241 nm are significantly lower than those previously used in many photochemical stratospheric modelling calculations. Acceptance of our cross sections in such models will affect markedly the calculated altitude profiles of ozone, nitrous oxide, chlorofluorocarbons, and other trace stratospheric species.

1. INTRODUCTION

We have recently performed high resolution photoabsorption cross section measurements of oxygen in the wavelength region 193-205 nm (Cheung et al., 1984a,b) with a 6.65 m photoelectric scanning spectrometer (Yoshino et al., 1980) of small enough instrumental band width to permit determination of the continuum cross section with minimal interference from the discrete Schumann-Runge bands (Yoshino et al., 1983, 1984) also present in this spectral region. In those studies of the absorption continuum, the interior of the 6.65 m spectrometer, after some changes (Cheung et al., 1984b), provided an optical path length of ~12 m, permitting the measurement of absorption cross sections as low as $\sim 10^{-23}$ cm^2 with oxygen pressures up to 760 torr, which corresponds to column densities up to $\sim 3 \times 10^{22}$ cm^{-2}. By studying the pressure dependence of the total cross section measured between the Schumann-Runge lines in this region, we were able to separate the pressure-independent component of the cross section, which contains the Herzberg continuum cross section of O_2, from the pressure-dependent component, which involves two molecules of O_2.

To extend the determination of the Herzberg continuum cross section of O_2 to its long wavelength threshold near 242 nm, it is necessary, with our photon-counting detection system, to use column densities of oxygen higher than those available in our previous experiments in the region 193-205 nm. Fortunately, at wavelengths greater than 204.7 nm, the intensity of the discrete Schumann-Runge absorption bands becomes negligible. Thus, the measurement of the weak Herzberg continuum cross section in the region 205-241 nm, which is a principal subject of this paper, does not require the use of high resolution. In the present work, the background continuum from a hydrogen discharge lamp is

dispersed by a small scanning monochromator and the monochromatic beam then passes into a multiple reflection cell providing optical path lengths up to 133 m for oxygen at pressures up to 760 torr. This multiple reflection cell is of unconventional design in that it was constructed by modifying the 6.65 m vacuum spectrometer/spectrograph. In brief, the concave grating was replaced by a set of ten small concave mirrors, and the plate-holder was replaced by a set of nine similar concave mirrors plus an integrated photoelectric detector. Details are given in Section 2.

By use of the technique outlined above, the continuous absorption cross section of oxygen has been studied in the region 202-241 nm as a function of path length and pressure of oxygen (Section 3.1). The measured cross section has been analyzed to yield the pressure-independent continuum and a pressure-dependent component (Section 3.2). In the present paper these results are combined with our previous results for the wavelengths 195-204 nm to give the Herzberg continuum cross section throughout the region 195-241 nm. Brief preliminary reports of this work have been given (Cheung et al., 1985).

The necessity for accurate laboratory determinations of the Herzberg continuum cross section and their significance for atmospheric photochemical modelling calculations have been recognized in several recent publications (Bucchia et al., 1985; Cheung et al., 1984a,b; Frederick et al., 1983; Nicolet, 1983; Brasseur et al., 1983; Crutzen and Schmailzl, 1983; Solomon et al., 1983; Ko and Sze, 1983; Jackman and Guthrie, 1983; National Research Council (U.S.), 1983; Froidevaux and Yung, 1982). Our cross section measurements are compared with those of others in Section 5.

2. EXPERIMENTAL PROCEDURE

2.1 Multiple reflection cell

To convert the 6.65 m vacuum spectrometer/spectrograph to a multiple reflection cell, the concave grating is replaced by an assembly of ten identical concave mirrors, each of 5 cm diameter and 6.65 m radius of curvature, and the plate-holder is replaced by an assembly of nine such mirrors and a stationary integrated photoelectric detector similar to that used in our photoelectric scanning attachment (Yoshino et al., 1980). In the assembly of ten mirrors, the one first receiving radiation from the entrance slit is located with its center on the optic axis of the 6.65 m instrument. The resultant multiple reflection cell, in which radiation focused on a mirror at one end of the cell is repeatedly refocused on an identical mirror at the other end and finally on the integrated detector, functions effectively as a modified White cell (White, 1942). This arrangement permits ten different optical path lengths, ranging from 133 to 13.3 m in decreasing steps of 13.3 m. The reason for constructing such an arrangement with its nineteen mirrors, instead of a White cell employing only two mirrors, is that the geometry of a White cell is incompatible with the fixed non-normal incident angle imposed by the geometry of the entrance slit compartment of the 6.65 m instrument. In the present reflection cell, each 13.3 m decrement in the optical path length is effected by eliminating one double pass in the cell; this is accomplished by readjusting a mirror located in the mount replacing the grating so that the radiation reflected from it is focused directly on the integrated detector instead of on a mirror in the mount bearing the detector.

Each of the mirrors in the present multiple reflection cell is independently adjustable about two axes to allow accurate alignment and focusing. Each mirror is specially coated (Acton Research Corp.) to enhance its reflectivity in the spectral region 205-235 nm. The measured reflectivities in this region are ~95%, so that even after nineteen reflections ~38% of the incident flux reaches the integrated detector. To prevent scattered radiation from entering the detector, a metal cylinder (2.5 cm internal diameter and 3.8 cm long) is positioned end-on in front of the integrated detector.

The path length, 6.65 m, between the mirrors at opposite ends of the multiple reflection cell was not measured directly, but was obtained from the accurately known radius of curvature, 6.65 m, of a concave grating used in zeroth order to focus radiation on the detector at the other end of the cell. The spectrometer grating and the assembly of ten mirrors are readily interchangeable in the 6.65 m instrument, each being attached to identical kinematic mounts; thus, the center of the grating and the center of the mirror first receiving radiation from the slit occupy identical positions in the 6.65 m instrument, thereby ensuring the accuracy of the path length determination.

2.2 Monochromator and optics

The continuous background for these photoabsorption cross section measurements of oxygen is provided by a d.c. hydrogen discharge lamp (Yoshino et al., 1983). This radiation passes directly through the entrance slit of a 0.3 m Czerny-Turner scanning vacuum monochromator (McPherson model 218) equipped with a 1200 line mm^{-1} grating blazed at

200 nm. Both mirrors and the grating in the monochromator were given the same highly reflective coatings (Acton Research Corp.) as were the mirrors in the multiple reflection cell. Wavelength calibration in the region 195-250 nm was performed by use of the Schumann-Runge bands (Yoshino et al., 1984) at the short wavelength end and the Herzberg I bands (Herzberg, 1952) at the long wavelength end. Wavelength accuracy is estimated to be ±0.1 nm. The instrumental full width at half maximum is ~0.13 nm with entrance and exit slit widths of 0.05 mm.

The monochromatic beam from the exit slit of the 0.3 m monochromator is focused by a silica lens (double convex, focal length 5 cm) onto the entrance of the multiple reflection cell, forming there an image of the source. The aperture of this lens is restricted so that a second silica lens (planoconvex, focal length 30 cm) placed close to the entrance of the cell forms an image, not larger than 5 cm in size, of this restricted aperture on that concave mirror (5 cm diameter) mounted on the optic axis at the opposite end of the cell. The restricted aperture (~2.4 mm) of the silica lens of focal length 5 cm ensures that radiation entering the multiple reflection cell first reaches only that particular concave mirror and none of its nine neighbors. This conclusion was verified experimentally.

To eliminate the possibility of interference by atmospheric absorption, all components of the apparatus (hydrogen discharge lamp, 0.3 m monochromator, silica lenses, and multiple reflection cell) were joined by evacuable couplings.

The initial alignment and focusing of the apparatus were facilitated by means of two helium-neon lasers, one positioned behind

the rear window of the hydrogen discharge lamp and the other positioned in place of the integrated detector.

2.3 Experimental conditions

The experimental conditions are summarized in Table 1. Although the total wavelength range covered is 195-245 nm, the present cross sections measured with low resolution are accurate only for wavelengths between 205 and 241 nm where discrete bands make a negligible contribution. The temperature of the oxygen inside the multiple reflection cell is monitored, to an accuracy of ±0.1 K, at one point inside the cell. During any particular scan the temperature changes by less than 0.3 K. The total range of temperatures for scans taken on different days is 296-300 K. This variation is insignificant in view of the observation (Johnston *et al.*, 1984) that the temperature dependence of the Herzberg continuum cross section of oxygen is negligible in the range 206-327 K. The oxygen gas used (Airco Industrial Gases, of stated purity 99.993%) was admitted to the multiple reflection cell without further purification. Pressures were measured with a capacitance manometer (MKS Baratron).

The optical depth of oxygen in the cell, $\ell n\ I_o/I$, is obtained from the measured ratio I_o/I of the signals transmitted with the cell empty (I_o) and filled (I). In practice, scans are made for a given path length at a series of pressures up to 760 torr, and the reference signal I_o is measured before and after such a series of measurements of I. Generally, the two values of I_o differ by only a few percent (otherwise, the series of scans is discarded); the value of I_o appropriate to a

particular scan with oxygen is obtained by interpolation on the assumption that the drift in I_o varies linearly with time. The whole procedure is then repeated for different path lengths.

3. EXPERIMENTAL RESULTS

3.1 Photoelectric scans of the cross section

Throughout the wavelength region 195-245 nm, photoelectric scans were performed first with a path length of 133 m, and subsequently with path lengths decreased in steps of 13.3 m, down to a final path length of 13.3 m. The accurately measured pressures at which the optical depth was scanned were selected from 13 pressures close to the values 5, 10, 20, 40, 60, 100, 160, 260, 360, 460, 560, 660 and 760 torr. For each of the path lengths 133.0, 119.7 and 106.4 m, scans were taken at all 13 pressures. For each of the path lengths 93.1, 79.8, 66.5 and 53.2 m, scans were taken at the 12 pressures above 5 torr. For each of the path lengths 39.9 and 26.6 m, scans were taken at the 11 pressures above 10 torr. For the path length 13.3 m, scans were taken at the 10 pressures above 20 torr. In summary, 119 scans were accumulated for 10 path lengths in the range 133-13.3 m and with 13 pressures of oxygen from 5 to 760 torr. In each scan the optical depth, and hence the cross section, were measured at wavelength intervals of 0.0167 nm throughout the region 195-245 nm.

A typical scan is illustrated in Fig. 1 where the total measured cross section for oxygen at 357 torr in a path length of 133 m is plotted against wavenumber in the wavelength region 244-198 nm. The absorption of oxygen is continuous between the weak Herzberg I bands, A $^3\Sigma_u^+$ - X $^3\Sigma_g^-$, at the low wavenumber end and the stronger Schumann-Runge bands, B $^3\Sigma_u^-$ - X $^3\Sigma_g^-$, at the high wavenumber end.

3.2 Analysis of the measured cross section of oxygen: $\sigma_P(\lambda)=\sigma_0(\lambda)+\alpha(\lambda)P$

The measured cross section is analyzed in terms of major contributions from the Herzberg continuum and the pressure-dependent continuum, variable contributions from the Schumann-Runge bands, if any, and minor contributions from Rayleigh scattering. Previous laboratory studies (e.g., Cheung et al., 1984a,b; Johnston et al., 1984) have shown that in this spectral region the total measured continuum cross section $\sigma_P(\lambda)$ is linearly dependent on the pressure P of oxygen:

$$\sigma_P(\lambda) = \sigma_0(\lambda) + \alpha(\lambda)P \qquad (1)$$

In Eq. (1), $\sigma_0(\lambda)$ is the cross section of O_2 extrapolated to zero pressure and $\alpha(\lambda)P$ is the cross section involving two molecules of O_2. The Herzberg continuum cross section $\sigma_H(\lambda)$ is obtained by subtracting from $\sigma_0(\lambda)$ the unwanted contribution $\sigma_{SR}(\lambda)$ of the Schumann-Runge bands at $\lambda < 204.7$ nm and the ubiquitous contribution $\sigma_R(\lambda)$ of Rayleigh scattering at all wavelengths. For $\lambda < 204.7$ nm, the wings of the Schumann-Runge bands may contribute to $\sigma_0(\lambda)$, and the intrinsic wing effects become magnified if insufficient spectroscopic resolution is used in measuring $\sigma_P(\lambda)$ between the Schumann-Runge lines. Our previous measurements at high resolution (0.0013 nm) between the absorption lines in the region 193.58-204.06 nm, assumed to be free of Schumann-Runge contributions in the paper by Cheung et al. (1984b), are adjusted in the present study for line-wing effects by a method given in Section 3.7. In the present work at low resolution (0.13 nm), $\sigma_P(\lambda)$ is studied at only two wavelengths less than 204.7 nm, viz., at 202.4 and 203.4 nm, at which the minor Schumann-Runge contributions are estimated by a method

given in Section 3.4. The Schumann-Runge bands are negligible in the main region, 205-241 nm, of the present work. Consequently, we may write

$$\sigma_0(\lambda) = \sigma_H(\lambda) + \sigma_{SR}(\lambda) + \sigma_R(\lambda) \qquad (2)$$

in which $\sigma_{SR}(\lambda)$ is zero for our low resolution measurements in the region 204.7 nm $\leq \lambda \leq$ 241.0 nm.

3.3 Cross section of oxygen in the region 205-241 nm

For the determination of $\sigma_0(\lambda)$ and $\alpha(\lambda)$ from our scans of $\sigma_P(\lambda)$, we select only those values of $\sigma_P(\lambda)$ with superior signal-to-noise characteristics. We have used Eq. (1) in this way to analyze the total continuum cross section at intervals of 1 nm throughout the region 205-241 nm, and the results are summarized in Section 3.5.

In Fig. 2 we show an example of the pressure dependence of the total continuum cross section at a particular wavelength, 220 nm, for 8 pressures in the range 100-760 torr. The various symbols in Fig. 2 indicate different path lengths and pressures which need not be specified here in detail. The scatter among the datum points is less at the higher pressures, and this result is generally true at other wavelengths. Nonetheless, in spite of the larger scatter of the datum points at the lower pressures, these points are valuable because our primary concern is with the value of the cross section σ_o, which corresponds to extrapolation to zero pressure. The straight line in Fig. 2 is a linear least squares fit of the data to Eq. (1). The

intercept σ_o = (4.18 ± 0.34)x10^{-24} cm^2 is the sum of the Herzberg continuum and Rayleigh scattering cross sections at 220 nm, and the gradient α = (0.89 ± 0.07)x10^{-26} cm^2 $torr^{-1}$ defines the pressure dependent continuum cross section at 220 nm.

The analysis of the pressure dependence of the total continuum cross section at 205 nm obtained with the present experimental arrangement with low resolution (0.13 nm) is of special interest because we have previously made unpublished measurements with high resolution (0.0013 nm) at 204.8 nm using the experimental arrangement described in our recent paper (Cheung et al., 1984b). In Fig. 3, the total continuum cross sections represented by the filled circles for pressures near 400, 500, 600 and 760 torr and for a path length of 11.89 m are from our high resolution work, whereas all the other symbols represent cross sections at various pressures and path lengths from the present work at low resolution. In particular, the symbols x from the present work correspond to the maximum path length of 133 m. In an effort to define better the extrapolation to zero pressure, we have obtained numerous points x at pressures below 200 torr. The dashed line in Fig. 3 is a linear least squares fit to the 4 points, represented by filled circles, obtained solely from our high resolution work, and yields σ_o = 5.5x10^{-24} cm^2 and α = 1.88x10^{-26} cm^2 $torr^{-1}$. The solid line in Fig. 3 is a linear least squares fit to all the data, obtained at high and low resolution, and yields σ_o = 7.21x10^{-24} cm^2 and α = 1.45x10^{-26} cm^2 $torr^{-1}$. The difference between the two linear fits clearly demonstrates the difficulty in obtaining a correct extrapolation to zero pressure from only the 4 filled circles corresponding to pressures of which the lowest is 400 torr. At the wavelength 205 nm relevant to Fig. 3, absorption by

the Schumann-Runge bands is negligible and the Schumann-Runge bands are not responsible for the difference between the two linear fits in Fig. 3. The existence of relatively many measurements at low pressures and long path lengths in the present work ensures that the solid line in Fig. 3 represents a much better extrapolation to zero pressure than the dashed line.

3.4 Cross section of oxygen in the region 202-205 nm

We believe that the extrapolation to zero pressure obtained by applying Eq. (1) to the cross section measurements at the longest two wavelengths, 203.21 and 204.06 nm, in our recent work with high resolution and limited column densities may be, by analogy with the dashed and solid lines in Fig. 3, subject to greater uncertainties than indicated in the values $\sigma_o(203.21\ nm) = (5.5 \pm 1.0)\times10^{-24}$ cm^2 and $\sigma_o(204.06\ nm) = (5.5 \pm 1.0)\times10^{-24}$ cm^2 given by Cheung et al (1984b). The more accurate values determined in the present work for $\lambda \geq 205$ nm decrease with increasing wavelength from the value σ_o (205 nm) = $(7.21 \pm 0.31)\times10^{-24}$ cm^2. This suggests that our previous σ_o values at 203.21 and 204.06 nm may require to be revised upwards. Direct comparison of these previous high resolution values of σ_o with the present low resolution results is not possible because, below 204.7 nm, contributions from the Schumann-Runge bands preferentially augment the low resolution results. In addition, and as expected, the wavelengths of the local minima in the measured cross section are, in the present low resolution work, shifted somewhat from the values obtained previously with high resolution.

We have examined, therefore, the pressure dependence of the present low resolution measurements at two local minima in the cross section, viz., at 202.4 and 203.4 nm, where contributions $\sigma_{SR}(\lambda)$ to the cross section occur from nearby Schumann-Runge bands mainly because of the low resolution used. In Figs. 4 and 5, all of the symbols except the filled circles represent the low resolution measurements at various path lengths and pressures, and, as in Fig. 3, the symbols x refer to low resolution measurements with a path length of 133 m. The filled circles are from our previous unpublished high resolution results at 202.4 nm and 203.4 nm. The solid lines in Figs. 4 and 5 are linear least squares fits to all of the low resolution data; these correspond to the values $\sigma_o = 7.89\times10^{-24}$ cm^2 and $\alpha = 1.54\times10^{-26}$ cm^2 torr^{-1} at 202.4 nm, and $\sigma_o = 7.63\times10^{-24}$ cm^2 and $\alpha = 1.53\times10^{-26}$ cm^2 torr^{-1} at 203.4 nm. To take into account the Schumann-Runge contributions at, for example, 202.4 nm, we have convolved our measured high resolution cross section of the discrete Schumann-Runge bands in the region 202.4 $\pm$ 0.13 nm with a triangular slit function having a full width at half maximum of 0.13 nm to obtain σ_{SR}(202.4 nm). This Schumann-Runge contribution amounts to 0.34×10^{-24} cm^2 at 202.4 nm, and a similar calculation produces a contribution of 0.43×10^{-24} cm^2 at 203.4 nm. The broken lines in Figs. 4 and 5 reflect (a) the subtraction of these Schumann-Runge band contributions from the solid line values that give the low resolution least squares fits, and (b) the assumption that the gradients of the least squares fits are unaltered. This assumption, which is equivalent to assuming that Schumann-Runge cross sections are independent of the pressure, has been verified in our previous studies (see Fig. 2 of Yoshino et al., 1983 and Fig. 3 of Cheung et al., 1984b). The reduced intercepts, σ_o(202.4 nm) = 7.55×10^{-24} cm^2 and σ_o(203.4 nm) = 7.20×10^{-24}

cm^2, and the corresponding values of α at these wavelengths replace the results given at 203.21 and 204.06 nm in Table 3 of Cheung et al. (1984b). The filled circles in Figs. 4 and 5, which represent our high resolution cross section measurements and which have not been used in obtaining the present linear least squares fits, are in good agreement with the dashed lines, i.e., with the low resolution cross sections after correction is made for instrumentally convolved contributions from nearby Schumann-Runge bands.

3.5 Values of $\sigma_0(\lambda)$ and $\alpha(\lambda)$ in the region 193.5-241.0 nm

Our final experimental values of $\sigma_0(\lambda)$ and $\alpha(\lambda)$ throughout the range 193.5-241.0 nm are listed in Table 2. The results in Table 2 for the range 193.58-202.08 nm include all of those in that region from Table 3 of our high resolution study (Cheung et al., 1984b) and three new high resolution results at 193.85, 195.34 and 196.40 nm. The results in Table 2 at 202.4 and 203.4 nm replace those at 203.21 and 204.06 nm in Table 3 of Cheung et al. (1984b), for the reasons given in Section 3.4. The results in Table 2 in the region 205.0-241.0 nm of pure continuum are from the present study, and the representative error estimates given at 5 nm intervals are significantly smaller than those for $\lambda < 205$ nm, where the accuracy of the extrapolation to zero pressure is adversely affected by the limited column densities available in our previous study at high resolution. In the region 194.4-202.1 nm, our experimental points for $\sigma_0(\lambda)$ and $\alpha(\lambda)$ from Cheung et al. (1984b) are shown in Figs. 6 and 7, respectively, together with empirically smoothed curves. For the region 203-241 nm, only the smoothed curves are shown

in Figs. 6 and 7 because our experimental values deviate insignificantly from the curves on the scales of Figs. 6 and 7.

3.6 Rayleigh scattering cross section of oxygen in the region 195-241 nm

Our cross sections $\sigma_0(\lambda)$ are derived from measurements of the total optical depth due to absorption and Rayleigh scattering (Eq. 2). To calculate the Rayleigh scattering cross section $\sigma_R(\lambda)$ of oxygen in the region 195-241 nm, we have used the formulae of Bates (1984), which are based on accurately measured refractivities and which take account of the wavelength dependence of the King correction factor. These $\sigma_R(\lambda)$ values decrease from 0.49×10^{-24} cm^2 at 195 nm to 0.15×10^{-24} cm^2 at 241 nm, and $\sigma_R(\lambda)$ is plotted at the bottom of Fig. 6. The ratios of $\sigma_R(\lambda)$ to our smoothed $\sigma_0(\lambda)$ values increase from 0.047 at 195 nm to 0.146 at 241 nm.

In an attempt to check the accuracy of Bates' formulae, we have measured optical depths in the region 195-240 nm in nitrogen with a path length of 133 m and pressures up to 760 torr. The resultant Rayleigh scattering cross sections of nitrogen are consistent with those calculated from Bates' formulae, but our poor signal-to-noise ratios for these low cross sections preclude a definitive test.

3.7 Schumann-Runge line-wing contributions to the continuum cross section of oxygen in the region 194.40-202.08 nm

Figure 6 shows the result of joining our accurate cross sections $\sigma_0(\lambda)$ in the region 205-241 nm of the pure continuum to those obtained for the continuum between the Schumann-Runge lines in the region 194.4-204.0 nm. The theoretical expectation for the shape of the Herzberg continuum is that it should resemble basically the shape of the v" = 0 probability amplitude, and, therefore, pass through a maximum (Section 4). Our results in Fig. 6 exhibit no such maximum in the region 194-241 nm. A possible explanation is that absorption to another excited state begins to contribute near 205 nm. However, such an explanation requires the additional absorption and that of the Schumann-Runge bands to have coincident wavelength thresholds. Therefore, we consider as more likely the possibility of contributions to the measured cross sections $\sigma_0(\lambda)$ from the line-wings of the Schumann-Runge bands, even though the instrumental band width used for these measurements between the lines is small (0.0013 nm).

In the region 194.4-202.1 nm, the Schumann-Runge lines are broadened by predissociation, especially at the shorter wavelengths (Yoshino et al., 1983 and 1984). The individual triplet components are incompletely resolved or unresolved (Cheung et al., 1986). Each spectral feature consists of overlapping broadened lines with wings extending considerably from line centers. We have made empirical fits to our observed Schumann-Runge spectral features that bracket the wavelength of the local minimum in the cross section between the line-complexes. By using one or more empirical Lorentzian line-profiles to fit each line-complex containing up to six overlapping Schumann-Runge

lines, we have determined the Lorentzian parameters and used them to calculate the wing contributions at the wavelength of interest. Initially, we have included Schumann-Runge line-complexes in the immediate neighborhood of these wavelengths; subsequently, we have added other more distant Schumann-Runge line-complexes until the additional calculated line-wing contributions become negligible. For the line-wing contribution at 193.58 nm arising from much broadened lines of the Schumann-Runge (4,0) band, this method was checked with a more elaborate computer program that performs spectral synthesis of Voigt lines from input which includes line center positions, triplet fine structure constants, band oscillator strengths, predissociation line widths, Doppler width, and instrumental band width. These two estimates of the wing contribution agree to within about 12%. We believe, therefore, that our Lorentzian estimates of the line-wing contributions $\sigma_{SR}(\lambda)$ present in our high resolution measurements are accurate to 15-20%.

The Schumann-Runge line-wing contributions (in 10^{-24} cm^2) to the continuum cross section measurements are given in parentheses following the wavelengths (in nm), which are listed in Table 2: 193.58 (9.6), 193.85 (7.1), 194.40 (5.6), 194.60 (6.3), 195.34 (12.1), 195.69 (3.8), 195.92 (2.4), 196.40 (4.4), 196.68 (1.7), 196.89 (1.3), 197.04 (1.1), 197.99 (0.88), 198.16 (0.60), 198.84 (0.22), 199.19 (0.09), 199.36 (0.09), 199.76 (0.33), 200.59 (0.22), 200.75 (0.21), 201.16 (0.04), 201.45 (0.03), 201.81 (0.02), 202.08 (0.02). In the region 193.5-205.0 nm the Schumann-Runge band oscillator strengths and predissociation line widths show an overall tendency to decrease with increasing wavelength and, <u>ceteris paribus</u>, the line-wing contributions reflect this.

Line-wing contributions to the $\sigma_0(\lambda)$ values obtained from our high resolution measurements are negligible at wavelengths greater than ~202 nm. The Herzberg continuum cross sections, $\sigma_H(\lambda)$, at the above wavelengths are obtained from Eq. (2), i.e., by subtracting the calculated line-wing contributions, $\sigma_{SR}(\lambda)$, and the calculated Rayleigh scattering cross sections (Section 3.6), $\sigma_R(\lambda)$, from the experimentally derived $\sigma_0(\lambda)$ values.

In Figure 8, all of our values of $\sigma_H(\lambda)$ in the region 193.5-204.1 nm are represented by open circles; the associated error bars are obtained from the quadratic combination of the estimated errors in $\sigma_0(\lambda)$ and $\sigma_{SR}(\lambda)$, since the additional contributions from possible errors in $\sigma_R(\lambda)$ are insignificant. The shape of the Herzberg continuum cross section in the wavelength region 194-204 nm is discussed further in Sections 4 and 5, but it is immediately apparent from a comparison of Fig. 6 and Fig. 8 that Schumann-Runge line-wings contribute significantly to the absorption cross section measured between the Schumann-Runge lines in the region 194-202 nm.

With the high resolution (0.0013 nm) used in the 194-204 nm region, we have shown (Yoshino et al., 1983) that the Schumann-Runge contributions $\sigma_{SR}(\lambda)$ are not degraded instrumentally. In contrast, the absorption cross sections described in Sec. 3.4 are measured with limited resolution (0.13 nm) and the contribution $\sigma_{SR}(\lambda)$ of the Schumann-Runge lines to the cross sections measured between them contained the effects of instrumental degradation.

4. CALCULATED HERZBERG CONTINUUM CROSS SECTION OF OXYGEN

According to the calculated cross sections in Fig. 1 of Saxon and Slanger (1986), which are based on the transition moments computed ab initio by Klotz and Peyerimhoff (1986), the fractional contribution of the Herzberg I continuum to the total continuum arising from the Herzberg I, II, and III transitions varies only a little, from ~0.8 to ~0.7, as the wavelength increases from 195 to 240 nm. Consequently, the shape of the measured (total) absorption cross section is expected to be not much different in this region from that of the Herzberg I continuum alone. In the following approximate treatment, we have taken the measured (total) absorption cross section from 205 to 237 nm, $\sigma_H(\lambda)$ in Table 3, as the Herzberg I, $A^3\Sigma_u^+ - X(0)\,^3\Sigma_g^-$, continuum cross section.

Our continuum cross section measurements are more accurate in the region 205-241 nm of pure continuum than in the region 195-205 nm where sometimes large line-wing contributions that are difficult to estimate must be subtracted, together with the Rayleigh scattering cross sections, from the cross sections measured between Schumann-Runge lines to yield the Herzberg continuum cross sections (Section 3.7). We decided, therefore, to use our measured Herzberg continuum cross section in the region 205-237 nm to generate a transition moment in this region. A short extrapolation of this effective transition moment to shorter wavelength then permits the calculation of the cross section in the region 195-205 nm, for comparison with our line-wing corrected continuum cross section measurements.

The absorption cross section $\sigma(\nu)$ at wavenumber ν for the transition from the bound ground state level v" = 0 to the dissociation

continuum of the upper A-state is given by (Allison et al., 1982)

$$\sigma(\nu) = k\nu[\int\psi'(R)D(R)\psi''(R)dR]^2 , \quad (3)$$

where $\psi'(R)$ is the upper state continuum wavefunction properly normalized with respect to its energy above the upper state dissociation limit, $\psi''(R)$ is the normalized v" = 0 wavefunction, and D(R) is the transition moment as a function of internuclear distance. In Eq. (3), $k = 8\pi^3/3$, and the units are the following: (au. a_0)$^{-\frac{1}{2}}$ for $\psi'(R)$, $a_0^{\frac{1}{2}}$ for $\psi''(R)$, ($a_0 e$) for D(R), and a_0 for R, in which au ($=e^2/a_0$) is the atomic unit (Hartree) of energy, e is the electronic charge and a_0 is the Bohr radius. The unit for the square of the matrix element in Eq. (3) is, therefore, a_0^3, so that Eq. (3) may be written in the form

$$\sigma(\lambda) = K\lambda^{-1}[\int\psi'(R)D(R)\psi''(R)dR]^2 , \quad (4)$$

with $\sigma(\lambda)$ in cm^2, λ in nm, and $K = 1.2253\times10^{-16}$. The application to Eq. (4) of the approximation that D(R) is linearly dependent on R, in the small relevant range of R, yields the equation (Jarmain and Nicholls, 1967)

$$K^{-1}\lambda q_{0,\lambda}^{\frac{1}{2}}\,\sigma(\lambda) = [D(\bar{R})]^2 \quad (5)$$

in which $q_{0,\lambda}$ is the Franck-Condon density for the overlap of the v" = 0 wavefunction with the A-state continuum wavefunction at wavelength λ, and $D(\bar{R})$ is the transition moment evaluated at the R-centroid, $\bar{R} = q_{0,\lambda}^{\frac{1}{2}}\int\psi'(R)R\psi''(R)dR$. Because $D(\bar{R})$ is a function of λ, we use also the approximation $D(\bar{R}) = A+B\lambda$ to determine the best least squares values of the constants A and B to fit values of $D(\bar{R})$ from Eq. (5), corresponding to our measured cross-sections and wavelengths, and calculated Franck-Condon densities, in the region 205-237 nm. The values found are $A = 1.317\times10^{-3}$ and $B = -2.865\times10^{-6}$. Details of the calculations of the potential functions and Franck-Condon densities are given in Appendix A.

The calculated transition moment decreases, per nm, by only ~0.39% of its value at 205 nm as the wavelength increases. Thus, its extrapolated value at 195 nm is only ~3.9% greater than its value at 205 nm. The calculated cross section for the region 190-237 nm is shown as the solid curve in Fig. 8.

5. HERZBERG CONTINUUM CROSS SECTION OF OXYGEN IN THE WAVELENGTH REGION 195-241 nm: EXPERIMENTAL LABORATORY AND STRATOSPHERIC DETERMINATIONS, AND CALCULATIONS

In Table 3 our values $\sigma_H(\lambda)$ for the Herzberg continuum cross section of oxygen are given. For the region 195-205 nm, we tabulate cross section values $\sigma_H(\lambda)$ corresponding to the extrapolated part of the curve in Fig. 8. For continuity, we tabulate $\sigma_H(\lambda)$ values corresponding to the curve from 205 to 210 nm, although the difference between the calculated and measured values is within experimental error. For wavelengths greater than 210 nm, the difference between the calculated and measured values is insignificant, and we arbitrarily exercise, in Table 3, our preference for the experimental values, for which representative error bars are shown at 5 nm intervals in Fig. 8. In the region 194-204 nm we show in Fig. 8 the line-wing corrected measured cross sections, $\sigma_H(\lambda) = \sigma_0(\lambda) - \sigma_{SR}(\lambda) - \sigma_R(\lambda)$, for comparison with our extrapolated calculated values. Despite the rather large experimental error bars we believe that these measurements provide support, in agreement with our calculation, for the existence of a maximum in the cross section near 201 nm.

In their Fig. 2, Saxon and Slanger (1986) show their calculated absorption cross section for the summed Herzberg I, II, and III transitions in the region 195-241 nm. They have multiplied the summed calculated cross section by 0.6 in their Fig. 2 in order to produce an approximate match with our experimental results in the region 205-241 nm, and its shape throughout the region 195-237 nm is similar to that of our calculated cross section in our Fig. 8. The continuity of the differential oscillator strength of the Herzberg I bands and Herzberg I continuum through the dissociation threshold near 242 nm is discussed in

Appendix B.

Table 3 shows also the recent laboratory results of Johnston et al. (1984) for oxygen at 297 K in the region 205-225 nm. They have ignored Rayleigh scattering and we list, therefore, the $\sigma_H(\lambda)$ values obtained from their $\sigma_0(\lambda)$ values and our calculated $\sigma_R(\lambda)$ values. In the region 205-225 nm investigated by Johnston et al., our Herzberg continuum cross sections and coefficients specifying the pressure dependence agree with theirs within the mutual errors of the determinations. In addition to their work at 297 K, Johnston et al. (1984) have studied the temperature dependence of the continuous absorption of oxygen in the region 205-225 nm for temperatures from 206 to 327 K. They find that, within their experimental error, the values of $\sigma_0(\lambda)$ and the product $\alpha(\lambda)T$ are independent of the temperature T.

Previous laboratory values of $\sigma_0(\lambda)$, and those from Table 2, are plotted in Fig. 6. For clarity, laboratory values of $\sigma_0(\lambda)$ and stratospheric values of $\sigma_H(\lambda)$ are the quantities shown in Fig. 6. Our laboratory values of $\sigma_0(\lambda)$ or $\sigma_H(\lambda)$ are as low as those of Johnston et al. (1984) in the region 205-225 nm that they have investigated, and are lower than all other previous laboratory values throughout the region 195-241 nm of our studies. Although the $\sigma_0(\lambda)$ values of Shardanand and Rao (1977) are higher than ours (Fig. 6), the agreement between our and their values of $\alpha(\lambda)$ is good (Fig. 7), presumably because their use of pressures in the range 1-25 atm causes $\alpha(\lambda)P$ rather than $\sigma_0(\lambda)$ to be the dominant contribution to their total measured cross section $\sigma_P(\lambda)$.

Table 3 and Fig. 6 include the four available sets of Herzberg continuum cross sections derived from measurements in the stratosphere.

In the in situ stratospheric determinations of Frederick and Mentall (1982), Herman and Mentall (1982), and Anderson and Hall (1983), the attenuation of solar radiation is measured, whilst in that of Pirre et al. (1984) the attenuation of stellar radiation is measured at night. In all of the published in situ determinations, the attenuation due to atmospheric Rayleigh scattering and ozone absorption is subtracted from the total to yield the Herzberg continuum cross section; the effects of Schumann-Runge line-wing contributions at wavelengths less than 205 nm are not estimated.

Frederick and Mentall (1982) present their results for the region 200-210 nm in the form of two sets of reduction factors by which the high laboratory cross section values of Hasson and Nicholls (1971a) or the lower values of Shardanand and Rao (1977) should be multiplied to produce consistency with the in situ measurements. We have translated these reduction factors to Herzberg cross sections in Table 3, where the reduced cross sections based on the laboratory results of Hasson and Nicholls (1971a) and Shardanand and Rao (1977) are given on the left and right sides, respectively, of the column headed FM. The former, which are plotted in Fig. 6, appear to be consistent with our $\sigma_H(\lambda)$ values, at least in the range 200-207 nm, but the absence of error estimates by Frederick and Mentall (1982) makes a more precise judgment difficult.

The stratospheric values of $\sigma_H(\lambda)$ found by Herman and Mentall (1982) for the region 200-220 nm are consistent with our laboratory values; their quoted errors are significantly greater than ours in the region 205-220 nm. In Fig. 6 our curve for $\sigma_0(\lambda)$ and the results of Herman and Mentall (1982) for $\sigma_H(\lambda)$ may be compared. Our curve for $\sigma_0(\lambda)$ shows a plateau corresponding to $\sigma_H(\lambda) = (6.8\text{-}7.0)\times10^{-24}$ cm^2 for

λ = 200-205 nm (Table 3), and a similar plateau with $\sigma_H(\lambda)$ = $(6.8\text{-}6.9)\times10^{-24}$ cm^2 for λ = 202-204 nm occurs in the results of Herman and Mentall (1982). However, the minimum they find near 206-208 nm and the maximum near 211 nm are not seen in our results.

Anderson and Hall (1983) have published, from stratospheric measurements, an average value of $\sigma_H(\lambda) = 7.0\times10^{-24}$ cm^2 for the region 203-207 nm. This value agrees well with ours, without the need to invoke much of their 30% error estimate. In more recent work, Hall and Anderson (1985) obtain an average cross section of $(6.9\pm1.0)\times10^{-24}$ cm^2 for the region 201-212 nm.

The only stratospheric values of $\sigma_H(\lambda)$ in serious conflict with the laboratory values in Table 3 are those of Pirre et al. (1984), who report cross sections for the region 202-220 nm. Their cross sections seem systematically and significantly higher than ours or those of Johnston et al. (1984). In the region 202-205 nm, the higher cross sections of Pirre et al. may be explicable in terms of unwanted contributions from Schumann-Runge bands, but in the region 205-214 nm their and our error bars do not overlap, although at longer wavelengths, 216-220 nm, their increasingly large error bars do permit overlap with ours.

6. CONCLUDING REMARKS

Our laboratory values of the Herzberg continuum absorption cross section of oxygen at room temperature are in good agreement with those of Johnston et al. (1984) in the wavelength region 205-225 nm covered by their investigation. In particular, our laboratory values are as low as those of Johnston et al. (1984) in the region 205-225 nm, and are lower than all other previous laboratory values throughout the region 195-241 nm of our studies. Our Herzberg continuum cross section given in Table 3 at intervals of 1 nm for the region 195-241 nm, increases from 6.3×10^{-24} cm^2 at 195 nm to a maximum of 6.6×10^{-24} cm^2 at 201 nm and then decreases to 0.85×10^{-24} cm^2 at 241 nm. Our values of the coefficients that define the linearly pressure-dependent cross section involving two molecules of oxygen are in good agreement with those of Johnston et al. (1984).

Four recent in situ stratospheric determinations of the Herzberg continuum cross section collectively span the region 200-220 nm. Our laboratory values are consistent with, but generally have smaller experimental errors than, the stratospheric values of Frederick and Mentall (1983), Herman and Mentall (1982), and Anderson and Hall (1983). Our results are in definite disagreement with the higher cross sections of Pirre et al. (1984), certainly in the region 205-214 nm.

The Herzberg continuum cross section calculated in the region 195-241 nm by Saxon and Slanger (1986) from the ab initio transition moment computations of Klotz and Peyerimhoff (1986) is, to within a scaling factor of 0.6 common to all wavelengths, in agreement (to within ~10%) with our Herzberg continuum cross section, which has been measured

accurately in the region 205-241 nm, and calculated and measured approximately in the region 195-205 nm. Our Herzberg continuum cross section in the region 195-241 nm is significantly lower than that previously used in many photochemical models of the stratosphere. The acceptance of our cross section in such calculations will affect markedly the results obtained for the altitude profiles of ozone, nitrous oxide, chlorofluorocarbons, and other trace stratospheric species.

Acknowledgements--We thank J.R. Esmond and N. Galluccio for technical assistance. We appreciate having received preprints of calculations by R.P. Saxon and T.G. Slanger, and by R. Klotz and S.D. Peyerimhoff. A.S.-C.C., K.Y., W.H.P., and D.E.F. are pleased to acknowledge support of this study by the Fluorocarbon Program Panel of the Chemical Manufacturers Association under Agreements FC82-412 and FC83-486 with Harvard University, and by the NASA Upper Atmospheric Research Program under Grant NAG5-484 to the Smithsonian Institution. S.L.G. gratefully acknowledges support of this research at ISR by the NASA Ames Cooperative Agreement NCC2-308 and at the Center for Astrophysics by the AFOSR Grant 84-0109 and NSF Grant ATM-83-12742; this research was also supported by a grant of computer time from the National Center for Atmospheric Research which is supported by the National Science Foundation.

REFERENCES

Allison, A.C. and Dalgarno, A. (1971) Continuity at the dissociation threshold in molecular absorption. J. chem. Phys. 55, 4342.

Allison, A.C., Guberman, S.L., and Dalgarno, A. (1982) Photoabsorption into the $^3\Pi_u$ state of O_2. J. geophys. Res. 87, 923.

Anderson, G.P. and Hall, L.A. (1983) Attenuation of solar irradiance in the stratosphere: Spectrometer results between 191 and 207 nm. J. geophys. Res. 88, 6801.

Bates, D.R. (1984) Rayleigh scattering by air. Planet. Space Sci. 32, 785.

Brasseur, G., DeRudder, A. and Simon, P.C. (1983) Implication for stratospheric composition of a reduced absorption cross section in the Herzberg continuum of molecular oxygen. Geophys. Res. Lett. 10, 20.

Bucchia, M., Megie, G., and Nicolet, M. (1985) Atmospheric transmittance and photodissociation rates in the 185-240 nm spectral range: Sensitivity of O_2 absorption cross sections in the Herzberg continuum and Schumann-Runge bands. Ann. Geophysicae 3, 429.

Cheung, A.S.-C., Yoshino, K., Parkinson, W.H. and Freeman, D.E. (1986) Molecular spectroscopic constants of $O_2(B\ ^3\Sigma_u^-)$, the upper state of the Schumann-Runge bands. J. mol. Spectrosc. (to be published).

Cheung, A.S.-C., Yoshino, K., Parkinson, W.H. and Freeman, D.E. (1985) Absorption cross section measurements of oxygen in the wavelength region 195-241 nm of the Herzberg continuum. Fortieth Symposium on Molecular Spectroscopy, Ohio State Univ., Abstract No. TC-5; and NASA Upper Atmospheric Programs Bulletin, No. 85-1, p. 10.

Cheung, A.S.-C., Yoshino, K., Parkinson, W.H. and Freeman, D.E. (1984a) Herzberg continuum cross section of oxygen in the wavelength region

193.5-204.0 nm: New laboratory measurements and stratospheric implications. Geophys. Res. Lett. 11, 580.

Cheung, A.S.-C., Yoshino, K., Parkinson, W.H. and Freeman, D.E. (1984b) Herzberg continuum cross section of oxygen in the wavelength region 193.5-204.0 nm and band oscillator strengths of the (0,0) and (1,0) Schumann-Runge bands. Can. J. Phys. 62, 1752.

Crutzen, P.J. and Schmailzl, U. (1983) Chemical budgets of the stratosphere. Planet. Space Sci. 31, 1009.

Frederick, J.E., Blake, A.J., Freeman, D.E., Nicholls, R.W., Ogawa, T. and Simon, P.C. (1983) Molecular absorption processes related to the penetration of ultraviolet solar radiation into the middle atmosphere, in Middle Atmosphere Program, Handbook for MAP, vol. 8, ed. C.F. Sechrist, Jr., pp. 53-74, ICSU Scientific Committee on Solar Terrestrial Physics, Urbana, Illinois.

Frederick, J.E. and Mentall, J.E. (1982) Solar irradiance in the stratosphere: Implications for the Herzberg continuum absorption of O_2. Geophys. Res. Lett. 9, 461.

Froidevaux, L. and Yung, Y.L. (1982) Radiation and chemistry in the stratosphere: Sensitivity to O_2 absorption cross sections in the Herzberg continuum. Geophys. Res. Lett. 9, 854.

Guberman, S.L. (1977) Accurate ab initio potential curve for the ground state of O_2. J. chem. Phys. 67, 1125.

Hall, L.A. and Anderson, G.P. (1985) personal communication.

Hasson, V. and Nicholls, R.W. (1971a) Absolute spectral absorption measurements on molecular oxygen 2640-1920 A: II. Continuum measurements 2430-1920 A. J. Phys. B (Atom. mol. Phys.) 4, 1789.

Hasson, V. and Nicholls, R.W. (1971b) Absolute spectral absorption measurements on molecular oxygen from 2640-1920 Å: I. Herzberg I

($A^3\Sigma_u^+ - X^3\Sigma_g^-$) bands (2640-2430 Å). J. Phys. B (Atom. mol. Phys.) 4, 1778.

Herman, J.R. and Mentall, J.E. (1982) O_2 absorption cross sections (178-225 nm) from stratospheric solar flux measurements. J. geophys. Res. 87, 8967.

Herzberg, G. (1952) Forbidden transitions in diatomic molecules. II. The $^3\Sigma_u^+ - ^3\Sigma_g^-$ absorption bands of the oxygen molecule. Can. J. Phys. 30, 185.

Jackman, C.H. and Guthrie, P.D. (1984) Sensitivity of N_2O, $CFC\ell_3$, and $CF_2C\ell_2$ two-dimensional distributions to O_2 absorption cross sections. J. geophys. Res. 90, 3919.

Jarmain, W.R. and Nicholls, R.W. (1967) A theoretical study of the v" = 0,1,2 progressions of bands and adjoining photodissociation continua of the Herzberg I system. Proc. phys. Soc. (London) 90, 545.

Johnston, H.S., Paige, M. and Yao, F. (1984) Oxygen absorption cross sections in the Herzberg continuum and between 206 and 327 K. J. geophys. Res. 89, 11661.

Klotz, R. and Peyerimhoff, S.D. (1986) Theoretical study of the intensity of the spin- or dipole-forbidden transitions between the c $^1\Sigma_u^-$, A' $^3\Delta_u$, A $^3\Sigma_u^+$ and X $^3\Sigma_g^-$, a $^1\Delta_g$, b $^1\Sigma_g^+$ states in O_2. Mol. Phys. (to be published).

Ko, M.K.W. and Sze, N.D. (1983) Effect of recent rate data revisions on stratospheric modeling. Geophys. Res. Lett. 10, 341.

Krupenie, P.H. (1972) The spectrum of molecular oxygen. J. phys. chem. Ref. Data 1, 423.

National Research Council (U.S.) (1984) Causes and Effects of Stratospheric Ozone Reduction: Update 1983. National Academy Press, Washington, D.C.

Nicolet, M. (1983) The influence of solar radiation on atmospheric chemistry. Ann. Geophysicae 1, 493.

Ogawa, M. (1971) Absorption cross sections of O_2 and CO_2 continua in the Schumann and far-uv regions. J. chem. Phys. 54, 2550.

Pirre, M., Rigaud, P. and Hugenin, D. (1984) New in-situ measurements of the absorption cross sections of O_2 in the Herzberg continuum. Geophys. Res. Lett. 11, 1199.

Saxon, R.P. and Slanger, T.G. (1986) Molecular oxygen absorption continua at 200-300 nm and O_2 radiative lifetimes. J. geophys. Res. (to be published).

Shardanand and Prasad Rao, A.D. (1977) Collision-induced absorption of O_2 in the Herzberg continuum. J. quant. Spectrosc. radiat. Transfer 17, 433.

Smith, A.L. (1971) Continuity of the differential oscillator strength through a dissociation limit; application to O_2 Schumann-Runge and Herzberg I systems. J. chem. Phys. 55, 4344.

Solomon, S., Rusch, D.W., Thomas, R.J. and Eckman, R.S. (1983) Comparison of mesospheric ozone abundances measured by the solar mesosphere explorer and model calculations. Geophys. Res. Lett. 10, 249.

White, J.U. (1942) Long optical paths of large aperture. J. opt. Soc. Am. 32, 285.

Yoshino, K., Freeman, D.E., Esmond, J.R. and Parkinson, W.H. (1983) High resolution absorption cross section measurements and band oscillator strengths of the (1,0)-(12,0) Schumann-Runge bands of O_2. Planet. Space Sci. 31, 339.

Yoshino, K., Freeman, D.E. and Parkinson, W.H. (1980) Photoelectric scanning (6.65 m) spectrometer for vuv cross section measurements.

Appl. Opt. 19, 66.

Yoshino, K., Freeman, D.E. and Parkinson, W.H. (1984) Atlas of the Schumann-Runge absorption bands of O_2 in the wavelength region 175-205 nm. J. phys. chem. Ref. Data 13, 207.

TABLE 1. EXPERIMENTAL CONDITIONS FOR THE PRESENT LOW RESOLUTION CROSS-SECTION MEASUREMENTS OF OXYGEN IN THE WAVELENGTH REGION 195-241 nm[a]

Total scan coverage	195-245 nm
Spectrometer bandwidth (FWHM)	0.13 nm
Spectrometer slit widths	0.05-0.02 nm
Individual scan intervals	50 nm
Continuous wavelength scan speed	0.083 nm/s
Period for accumulating counts	0.200 s
Interval between datum points	0.0167 nm
Number of datum points per scan	~3000
Temperature	296-300 K
Optical path length	13.3-133 m
Pressure range	5-760 torr

[a]The analogous conditions for our high resolution cross section measurements in the region 193.5-204.0 nm are given in Table 2 of Cheung et al. (1984b).

TABLE 2. PRESENT LABORATORY VALUES OF THE CONTINUOUS CROSS-SECTION OF OXYGEN AT 296-300 K AND ITS PRESSURE DEPENDENCE IN THE WAVELENGTH REGION 193.5-241.0 nm OF THE HERZBERG CONTINUUM[a]

λ	$\sigma_o(\lambda)$[b]	$\alpha(\lambda)$	λ	$\sigma_o(\lambda)$	$\alpha(\lambda)$	λ	$\sigma_o(\lambda)$	$\alpha(\lambda)$
193.58	14.2±0.9	2.44±0.30	202.4[c]	7.55±0.31	1.54±0.10	226.0	3.01	0.67
193.85	13.3±1.1	2.44±0.30	203.4[c]	7.20±0.31	1.53±0.10	227.0	2.82	0.63
194.40	11.8±0.8	2.43±0.29	205.0[d]	7.21±0.31	1.45±0.08	228.0	2.62	0.60
194.60	11.8±0.8	2.43±0.29	206.0	7.08	1.40	229.0	2.44	0.57
195.34	17.2±1.2	2.40±0.35	207.0	6.93	1.36	230.0	2.26±0.30	0.54±0.06
195.69	9.8±0.6	1.90±0.15	208.0	6.65	1.33	231.0	2.13	0.51
195.92	9.8±0.6	1.90±0.14	209.0	6.44	1.30	232.0	1.99	0.48
196.40	11.9±1.0	2.10±0.35	210.0	6.20±0.34	1.27±0.08	233.0	1.85	0.45
196.68	9.3±0.9	1.90±0.14	211.0	5.98	1.24	234.0	1.67	0.43
196.89	9.0±0.8	1.90±0.14	212.0	5.82	1.20	235.0	1.57±0.31	0.40±0.07
197.04	9.0±0.8	1.90±0.15	213.0	5.69	1.15	236.0	1.50	0.36
197.99	8.5±0.7	1.80±0.20	214.0	5.52	1.10	237.0	1.34	0.35
198.16	8.0±0.7	1.86±0.19	215.0	5.31±0.33	1.06±0.07	238.0	1.21	0.33
198.84	7.8±0.7	1.86±0.20	216.0	5.04	1.04	239.0	1.19	0.29
199.19	7.5±0.7	1.63±0.20	217.0	4.78	1.01	240.0	1.11±0.30	0.27±0.06
199.36	7.5±0.7	1.63±0.20	218.0	4.60	0.97	241.0	1.00	0.25
199.76	7.5±0.6	1.63±0.20	219.0	4.36	0.94			
200.59	7.3±0.7	1.67±0.19	220.0[d]	4.18±0.34	0.89±0.07			
200.75	7.3±0.7	1.67±0.18	221.0	3.96	0.86			
201.16	6.8±0.7	1.56±0.25	222.0	3.74	0.82			
201.45	6.8±0.7	1.56±0.25	223.0	3.59	0.78			
201.81	6.8±0.7	1.56±0.25	224.0	3.45	0.73			
202.08	6.8±0.7	1.62±0.24	225.0	3.21±0.31	0.70±0.07			

[a] The continuous cross section is $\sigma_P(\lambda) = \sigma_o(\lambda) + \alpha(\lambda)P$, in which $\sigma_o(\lambda)$ is given by Eq. (2) and P is the range 5-760 torr. The units for $\lambda, \sigma_o(\lambda)$ and $\alpha(\lambda)$ are nm, 10^{-24} cm^2 and 10^{-26} cm^2 torr^{-1}, respectively. In the region 205-241 nm, representative error estimates for $\sigma_o(\lambda)$ and $\alpha(\lambda)$ are given at 5 nm intervals.

[b] For $\lambda < 202$ nm, $\sigma_0(\lambda)$ obtained from our high resolution measurements contains intrinsic line-wing contributions $\sigma_{SR}(\lambda)$ estimated in Section 3.7 of the text.

[c] σ_0(202.4 nm) and σ_0(203.4 nm) obtained from our low resolution measurements after removal of line-wing contributions due to limited resolution (see Section 3.4 of the text).

[d] See Section 3.3 of the text.

TABLE 3. HERZBERG CONTINUUM ABSORPTION CROSS SECTION, $\sigma_H(\lambda)$ IN 10^{-24} cm^2, OF OXYGEN IN THE WAVELENGTH REGION 195-241 nm

λ	Laboratory values		Stratospheric values				
	Present study[a,b]	Johnston et al. (1984)[c]	FM[d]		HM[e]	AH[f]	PRH[g]
195	6.26						
196	6.38						
197	6.45						
198	6.53						
199	6.57						
200	6.59		7.2	9.4	7.8		
201	6.62		7.1	9.2	7.3		
202	6.61		6.9	8.9	6.9		10.2
203	6.58		7.7	8.6	6.9	7.0	
204	6.55		7.5	8.3	6.8	7.0	9.8
205	6.50	7.0	7.3	7.8	6.5	7.0	
206	6.43		7.1	7.4	6.3	7.0	9.8
207	6.35		7.0	7.2	6.3	7.0	
208	6.24		7.8	7.3	6.3		8.8
209	6.11		7.6	7.1	6.5		
210	5.89	6.6	7.4	6.9	6.7		8.5
211	5.68				6.7		
212	5.53				6.4		8.0
213	5.40				6.2		
214	5.24				6.0		8.0
215	5.04	4.7			5.8		
216	4.78				5.5		7.1

217	4.52		5.1	
218	4.35		5.1	6.7
219	4.11		4.9	
220	3.94	4.5	4.4	4.8
221	3.73			
222	3.51			
223	3.37			
224	3.23			
225	3.00	2.8		
226	2.80			
227	2.62			
228	2.42			
229	2.25			
230	2.07			
231	1.95			
232	1.81			
233	1.67			
234	1.50			
235	1.40			
236	1.33			
237	1.18			
238	1.05			
239	1.03			
240	0.96			
241	0.85			

[a] The temperature is 296-300 K.

[b] For $\lambda \geq 210$ nm, the experimental values $\sigma_H(\lambda) = \sigma_0(\lambda) - \sigma_R(\lambda)$, obtained with low resolution, are listed. For $\lambda < 210$ nm, our calculated values

are listed, corresponding to the solid curve of Fig. 8; see Sections 3.7 and 4 of the text.

[c] We obtain $\sigma_H(\lambda)$ by subtraction of our calculated Rayleigh scattering cross sections (Section 3.6) from the cross sections given for the temperature 297 K in Table 1 of Johnston et al. (1984).

[d] FM: Frederick and Mentall (1982). The left and right columns below correspond, respectively, to the columns headed $c_\lambda(O_2)^1$ and $c_\lambda(O_2)^2$ in Table 2 of their paper.

[e] HM: Herman and Mentall (1982). Their quoted errors are 0.8 to 0.6 x 10^{-24} cm^2 from 200 to 215 mm, and 0.9 x 10^{-24} cm^2 at 220 nm.

[f] AH: Anderson and Hall (1983). Their quoted errors are 2.0 x 10^{-24} cm^2.

[g] PRH: Pirre, Rigaud and Hugenin (1984). Their quoted errors increase from 0.9 x 10^{-24} cm^2 at 202 nm to 4.1 x 10^{-24} cm^2 at 220 nm.

APPENDIX A: CALCULATED POTENTIALS FOR THE A $^3\Sigma_u^-$ AND $X^3\Sigma_g^-$ STATES OF O_2, AND FRANCK-CONDON DENSITIES FOR THE A-X(0) TRANSITION

To calculate the Franck-Condon densities for Eq. (5), the excited A $^3\Sigma_u^+$ and ground X $^3\Sigma_g^-$ state potentials are needed. Both potential curves and their associated vibrational wavefunctions were obtained on a grid of 2000 points between 0.0 and 4.2 Å. The potential curves described below were fitted by cubic splines. The vibrational wavefunctions were calculated by solving numerically the one-dimensional radial Schrödinger equation by the Numerov method for the bound and continuum wavefunctions. The Franck-Condon factors and densities were determined by use of the trapezoidal rule.

For the A $^3\Sigma_u^+$ state, 94 points were used for the cubic spline fit. 44 of these points, between 1.301 and 2.423 Å, were taken from the Rydberg-Klein-Rees (RKR) data listed by Krupenie (1972). 12 points required to define the repulsive wall were added for R < 1.301 Å. These points were determined, from ab initio calculations in a [3s, 2p, 1d] Gaussian basis set, by an approach similar to that described previously (Guberman, 1977). Multiconfigurational self-consistent field (MCSCF) calculations were used to determine orbitals for the ground state. With the ground state orbitals, a first order configuration interaction (CI) wavefunction was constructed for the A $^3\Sigma_u^+$ state. The CI wavefunction was generated by taking all double excitations to the full virtual orbital space from a multireference set of configurations needed for the proper dissociation of the A $^3\Sigma_u^+$ state. No configuration was allowed to have more than a single electron in the virtual orbitals. This procedure led to a CI wavefunction with 2386 terms for the A $^3\Sigma_u^+$ state, for which the calculated

energies are shown in Table A1. The energies and internuclear distances given in Table A1 were shifted to align the calculated repulsive wall with the inner wall of the potential well given by the RKR points. The resulting shifted points are shown in Table A2. For R > 2.423 Å, additional points were added, out to the asymptote at 6649 cm^{-1}. The Franck-Condon factors obtained here are not sensitive to the precise shape of the potential curve in this region. The added points were based on a quadratic interpolation between ab initio results for the A' $^3\Delta_u$ state (S.L. Guberman, unpublished results), which is nearly degenerate with the A $^3\Sigma_u^+$ state in this region.

The X $^3\Sigma_g^-$ ground state potential came from Krupenie (1972) and was supplemented at large internuclear distances by ab initio results (Guberman, 1977).

TABLE A1: CALCULATED CI ENERGIES FOR O_2 ($A\ ^3\Sigma_u^+$)

R[a]	E[b]
1.9	-0.28806
2.0	-0.40503
2.1	-0.49053
2.2	-0.55261
2.2819	-0.59023
2.4	-0.62886
2.42	-0.63393
2.44	-0.63863
2.46	-0.64299
2.48	-0.64703
2.50	-0.65076
2.52	-0.65420

[a] Internuclear distances R are in atomic units of $a_0 = 0.52918 \times 10^{-8}$ cm.

[b] Energies E are in Hartree (1 Hartree = 27.21165 eV). Add -149.0 to each energy to get the total energy.

TABLE A2: REPULSIVE WALL ENERGIES FOR O_2 ($A\ ^3\Sigma_u^+$)

R[a]	E[b]
0.9589	87509.00
1.0118	61835.00
1.0647	43072.00
1.1176	29450.16
1.1610	21192.26
1.2235	12714.99
1.2340	11602.44
1.2446	10569.93
1.2552	9612.82
1.2658	8727.04
1.2764	7908.42
1.2870	7153.47

[a] Internuclear distances R are in Å.

[b] Energies E are in cm^{-1}. The zero of energy is the minimum in the RKR curve given by Krupenie (1972).

APPENDIX B: CONTINUITY OF THE DIFFERENTIAL OSCILLATOR STRENGTH AT THE DISSOCIATION THRESHOLD OF THE HERZBERG I SYSTEM OF O_2

The general case of the continuity of the differential oscillator strength through a dissociation limit has been considered quantum mechanically by Allison and Dalgarno (1971) and semi-classically by Smith (1971). The results of the two treatments are in essential agreement, provided that in the semi-classical formulation the WKB approximation for the continuum state is not used too close to the dissociation threshold. Smith (1971) has applied the continuity relationship to earlier data on the Herzberg I bands and Herzberg continua.

Measurements of the continuum cross section of O_2 in the region 195-242 nm include contributions from the A-X (Herzberg I), c-X (Herzberg II),and A'-X (Herzberg III) continua. Estimation of the relative cross sections of these transitions from the calculated curves in Fig. 1 of Saxon and Slanger (1986), which are based on the transition moments computed by Klotz and Peyerimhoff (1986), reveals that the fractional contribution of the A-X continuum to the total calculated cross section decreases monotonically from ~0.80 at 215 nm to ~0.69 at 240 nm. We assume that the calculated cross sections of Saxon and Slanger (1986) for the Herzberg I, II, and III continua are determined better to within a common scaling factor at a given wavelength than absolutely. We have examined graphically the continuity relationship between the Herzberg I band oscillator strengths of Hasson and Nicholls (1971b), which are the latest available, and the Herzberg I continuum cross section in the region 215-240 nm, obtained by multiplying our measured (total) absorption continuum cross section (σ_H in Table 3) by factors (between 0.80 and 0.69) estimated from Fig. 1 of Saxon and Slanger (1986). These graphical results violate the

continuity relationship. Increases of about 20% in the Herzberg I band oscillator strengths of the (7,0)-(10,0) bands of Hasson and Nicholls (1971b) produce significantly improved continuity. The experimental determination of the Herzberg I band oscillator strengths is difficult because the bands are very weak and sharp. Hasson and Nicholls (1971b) estimate errors in the band oscillator strengths of ±15% for the (7,0) and (8,0) bands, and ±20% for the (9,0) and (10,0) bands. However, the systematic increases of ~20% indicated by the continuity relationship suggest that a new experimental determination of the Herzberg I band oscillator strengths may be desirable.

Figure Captions

Fig. 1 Absorption cross section of oxygen at 357 torr in a path length of 133 m, plotted against wavenumber in the wavelength region 244-198 nm. Absorption is continuous between the Herzberg I bands A-X and the Schumann-Runge bands B-X. See Section 3.1 of the text.

Fig. 2 Continuum cross section $\sigma_P(\lambda)$ of oxygen at λ = 220 nm as a function of oxygen pressure. See Section 3.3 of the text.

Fig. 3 Continuum cross section $\sigma_P(\lambda)$ of oxygen at λ = 205 nm as a function of oxygen pressure. Points represented by filled circles are from high resolution data with P $\geq\sim$400 torr; other points are from low resolution data with P $\geq\sim$20 torr. The two linear extrapolations to zero pressure are discussed in Section 3.3 of the text.

Fig. 4 Cross section $\sigma_P(\lambda)$ of oxygen at λ = 202.4 nm as a function of oxygen pressure. Points represented by filled circles are from high resolution data; other points are from low resolution data. The upper and lower linear extrapolations to zero pressure correspond, respectively, to the presence and removal of contributions $\sigma_{SR}(\lambda)$ of Schumann-Runge bands to $\sigma_P(\lambda)$. See Section 3.4 of the text.

Fig. 5 Cross section $\sigma_P(\lambda)$ of oxygen at λ = 203.4 nm as a function of oxygen pressure. Points represented by filled circles are from high resolution data; other points are from low resolution data. The upper and lower linear extrapolations to zero pressure correspond, respectively, to the presence and removal of contributions $\sigma_{SR}(\lambda)$ of Schumann-Runge bands to $\sigma_P(\lambda)$. See Section 3.4 of the text.

Fig. 6 Continuum cross section of oxygen plotted against wavelength in the region 194-241 nm. The ordinate is the Herzberg continuum cross section $\sigma_H(\lambda)$ for the stratospheric results, which are represented

by filled symbols. For clarity, the ordinate is $\sigma_0(\lambda)$ [$=\sigma_H(\lambda)$ + $\sigma_{SR}(\lambda)$ + $\sigma_R(\lambda)$] for the laboratory results, which are represented by open symbols and stars. The calculated Rayleigh scattering cross section of O_2, $\sigma_R(\lambda)$, is plotted at the bottom of the Figure. See Sections 3.5-3.7 and 4 of the text.

Fig. 7 The coefficient $\alpha(\lambda)$, specifying the cross section $\alpha(\lambda)P$ involving two molecules of oxygen, plotted against wavelength in the region 194-241 nm. See Section 3.5 of the text.

Fig. 8 Our experimental and calculated Herzberg continuum cross section, $\sigma_H(\lambda)$, of O_2. The open circles represent $\sigma_H(\lambda)$ measured with high resolution between Schumann-Runge lines in the region 193.5-205.0 nm, after subtraction of contributions from line-wings, $\sigma_{SR}(\lambda)$, and Rayleigh scattering, $\sigma_R(\lambda)$. The asterisks in the region 205-241 nm represent $\sigma_H(\lambda)$ measured with low resolution, after subtraction of $\sigma_R(\lambda)$; for the asterisks representing $\sigma_H(\lambda)$ at 202.4 and 203.4 nm, see Section 3.4. The solid curve represents our calculated Herzberg I continuum designed to fit our measured (total) $\sigma_H(\lambda)$ in the region 205-237 nm, and extrapolated to the region 195-205 nm (see Sections 4 and 5 of the text).

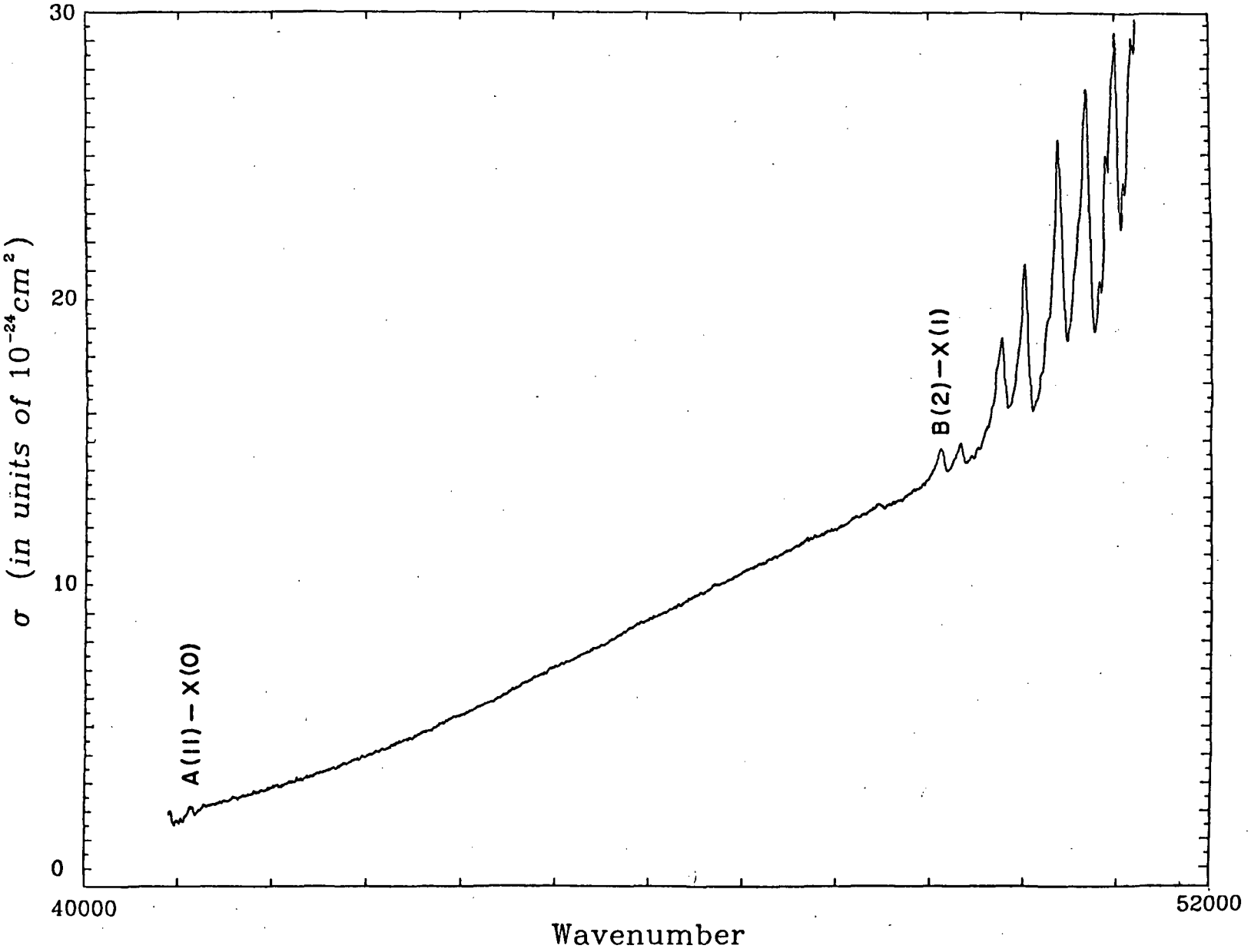
30
20
10
0
σ (in units of $10^{-24} cm^2$)
A(11) – X(0)
B(2) – X(1)
40000
52000
Wavenumber

Fig. 1

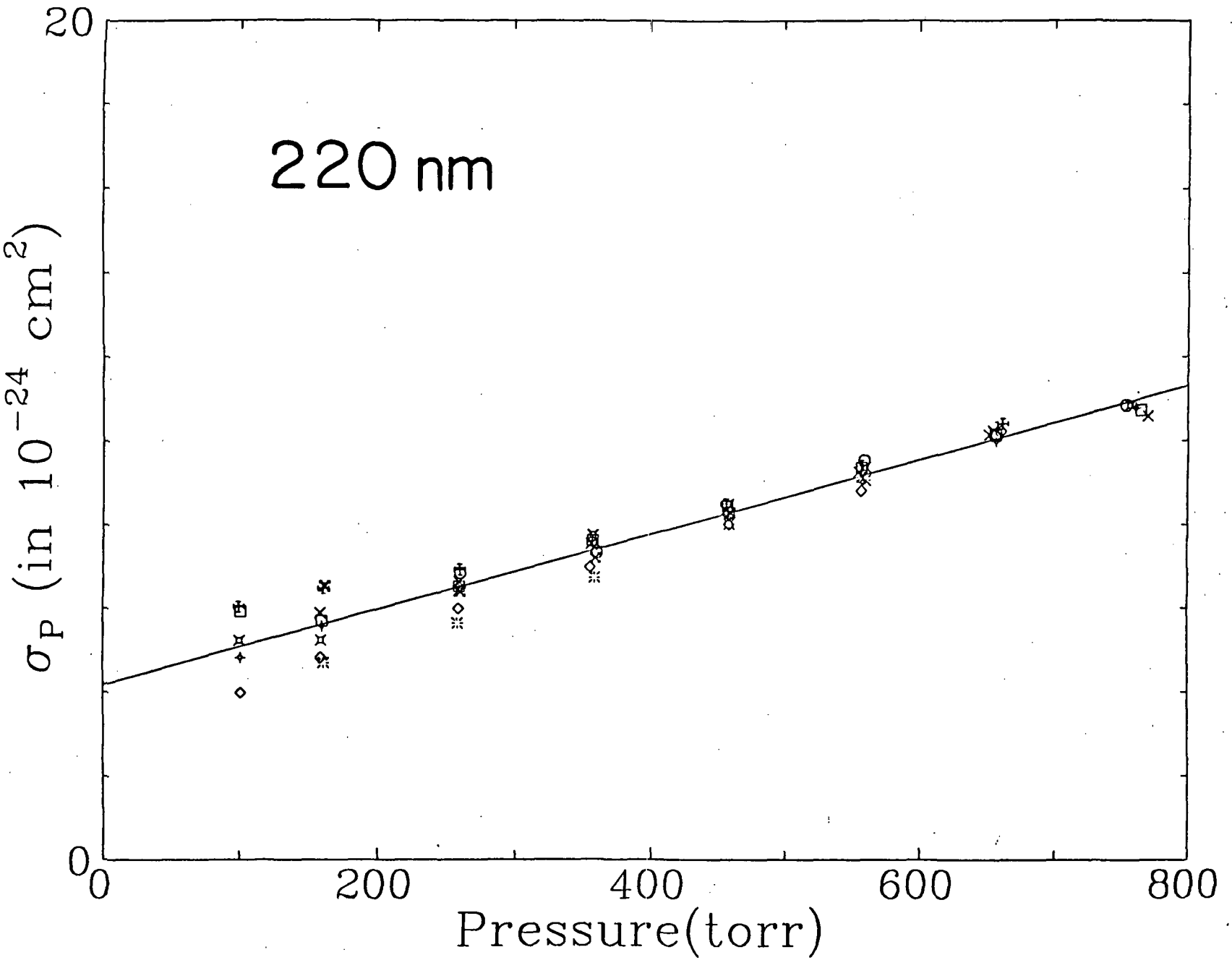

Fig. 2

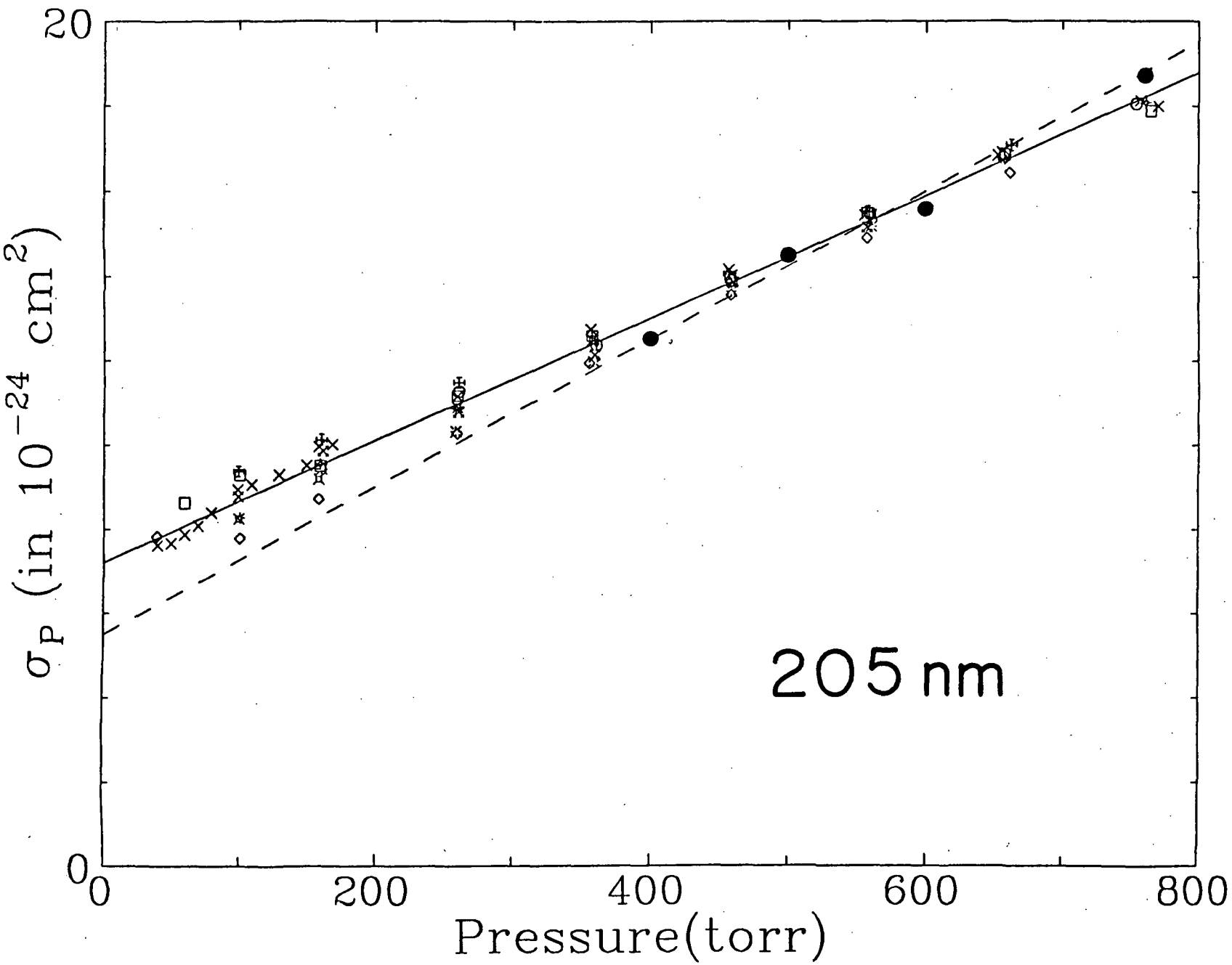

Fig. 3

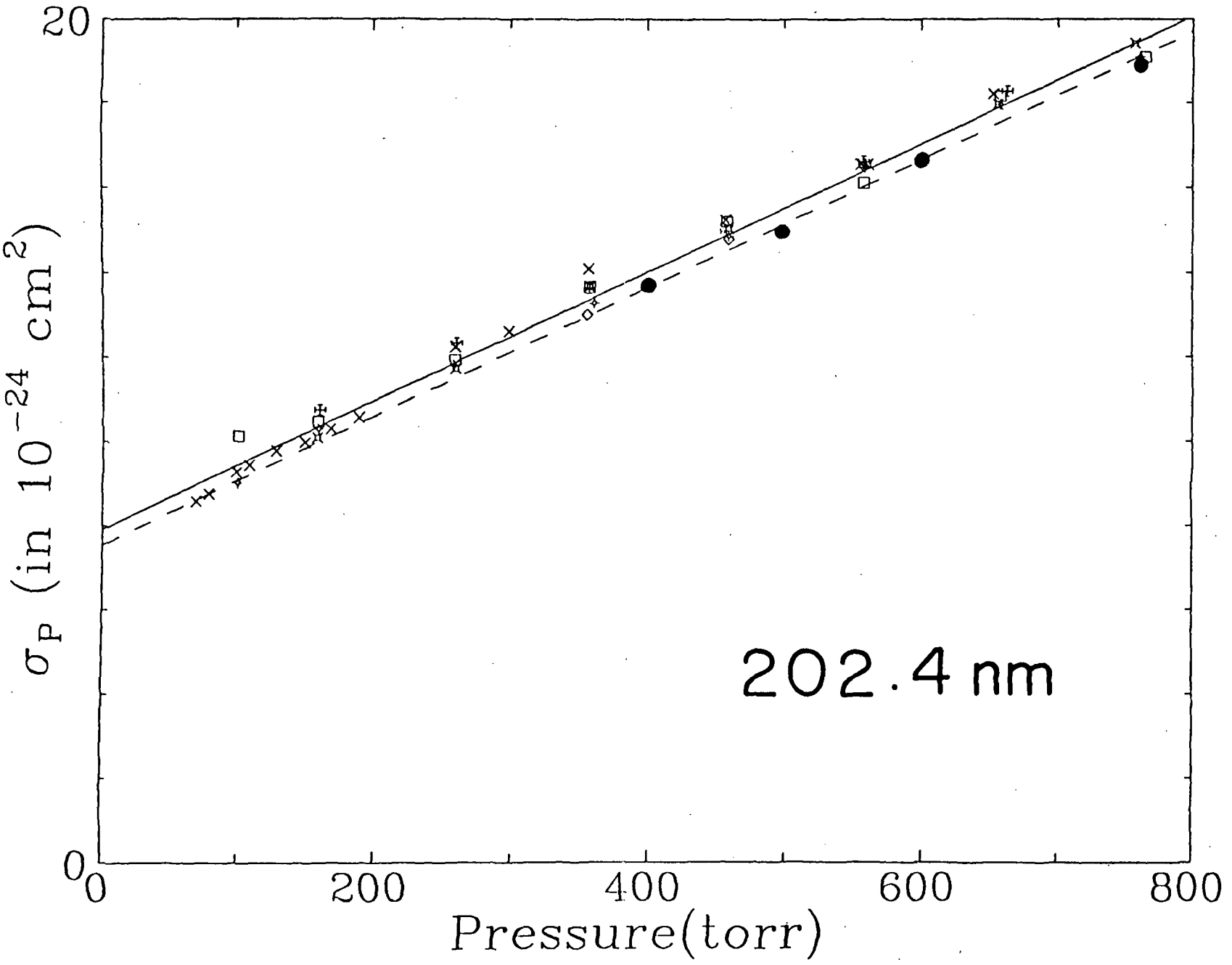

Fig. 4

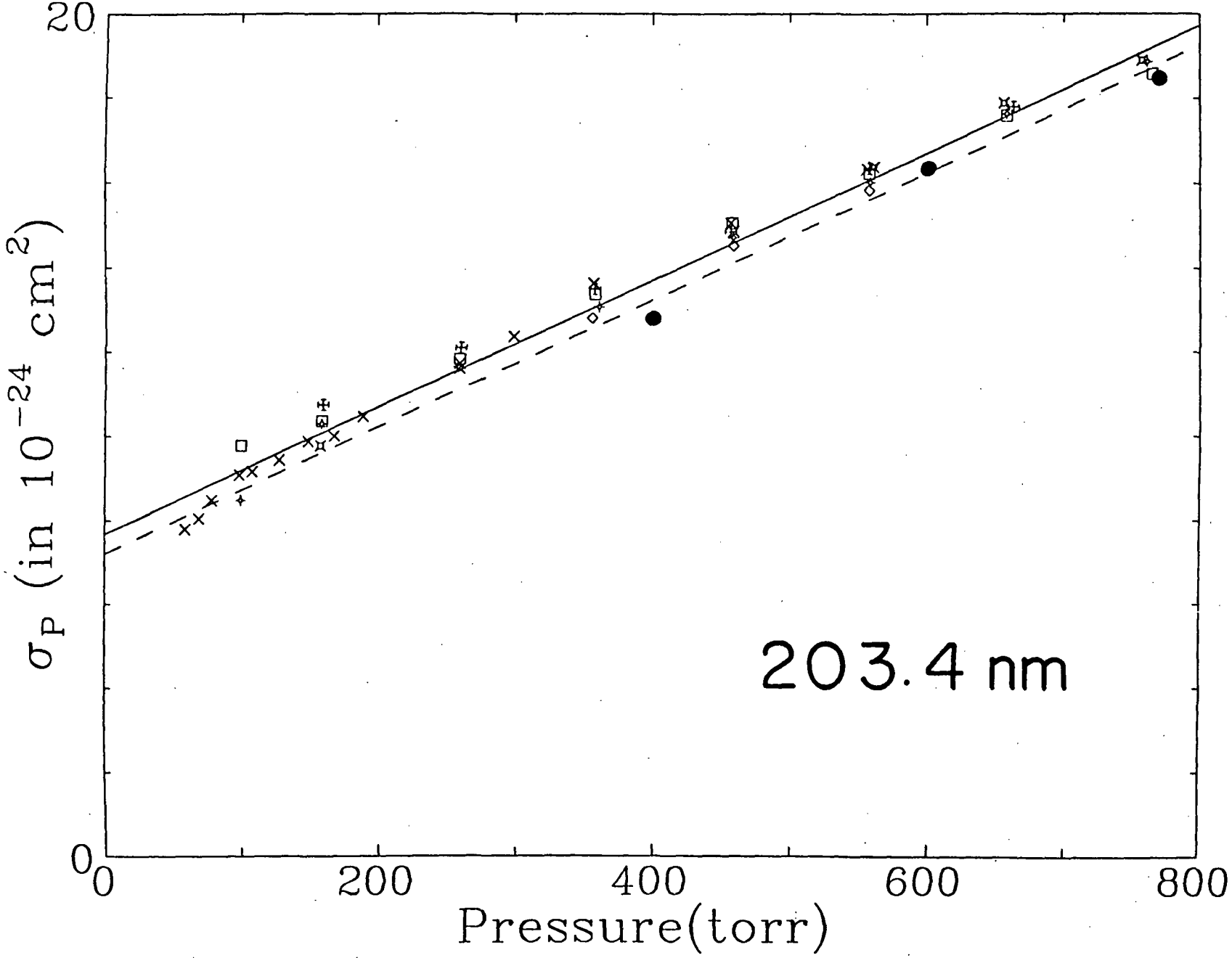

Fig. 5

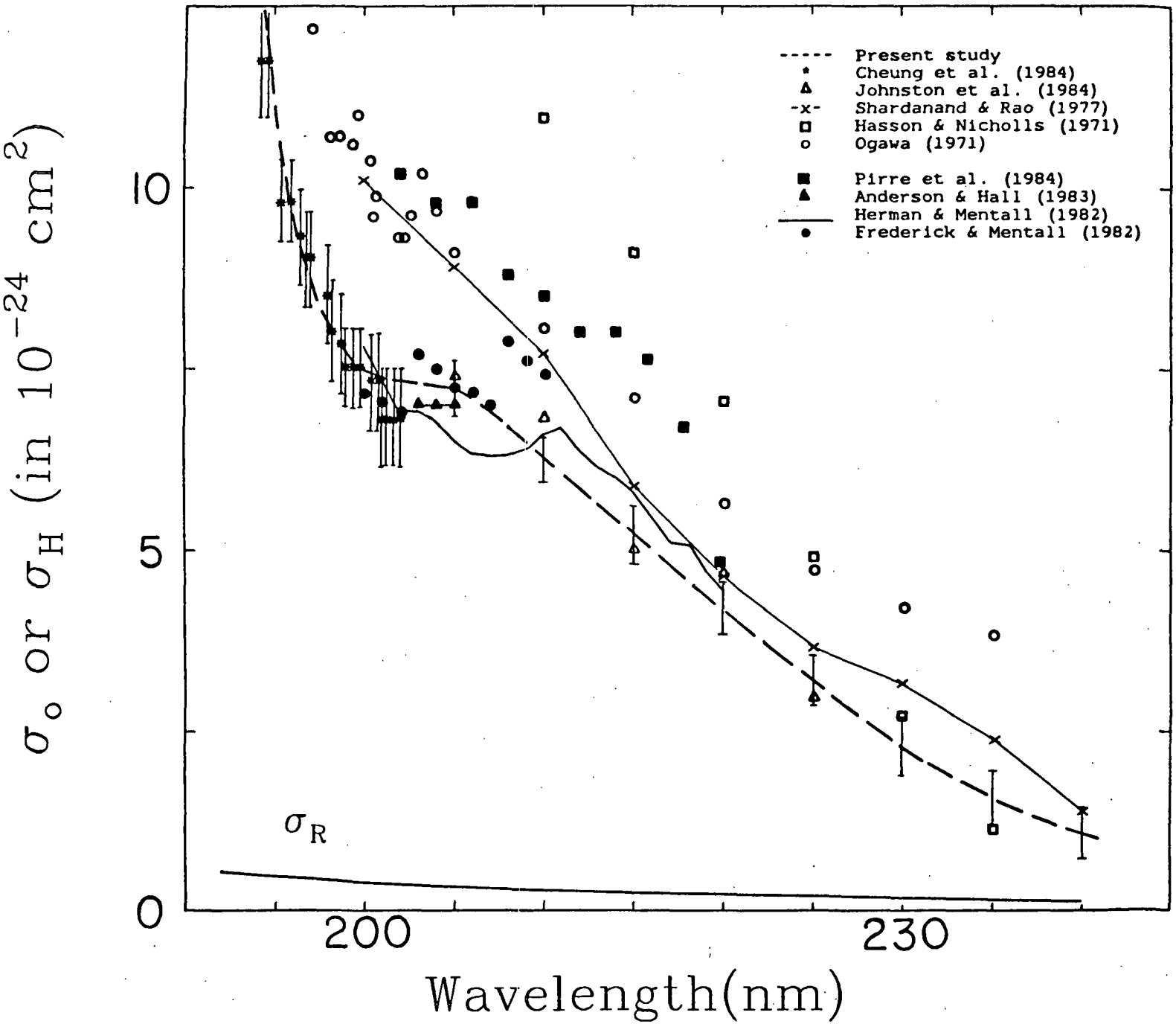
Present study
Cheung et al. (1984)
Johnston et al. (1984)
Shardanand & Rao (1977)
Hasson & Nicholls (1971)
Ogawa (1971)
Pirre et al. (1984)
Anderson & Hall (1983)
Herman & Mentall (1982)
Frederick & Mentall (1982)
σ_R
σ_o or σ_H (in 10^{-24} cm^2)
0
5
10
200
230
Wavelength(nm)

Fig. 6

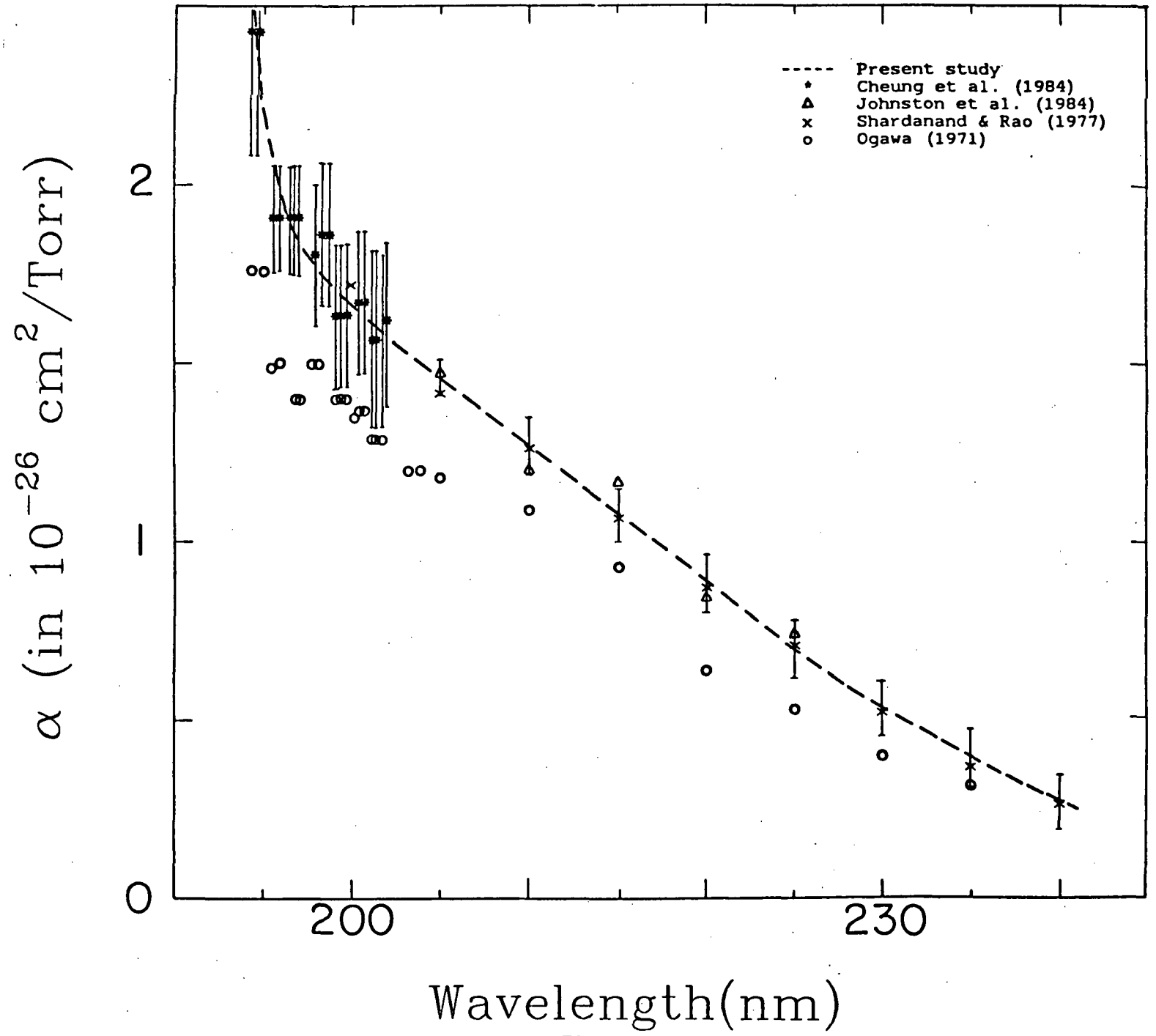
----- Present study
* Cheung et al. (1984)
Δ Johnston et al. (1984)
x Shardanand & Rao (1977)
o Ogawa (1971)
α (in 10^{-26} cm^2/Torr)
0
1
2
200
230
Wavelength(nm)

Fig. 7

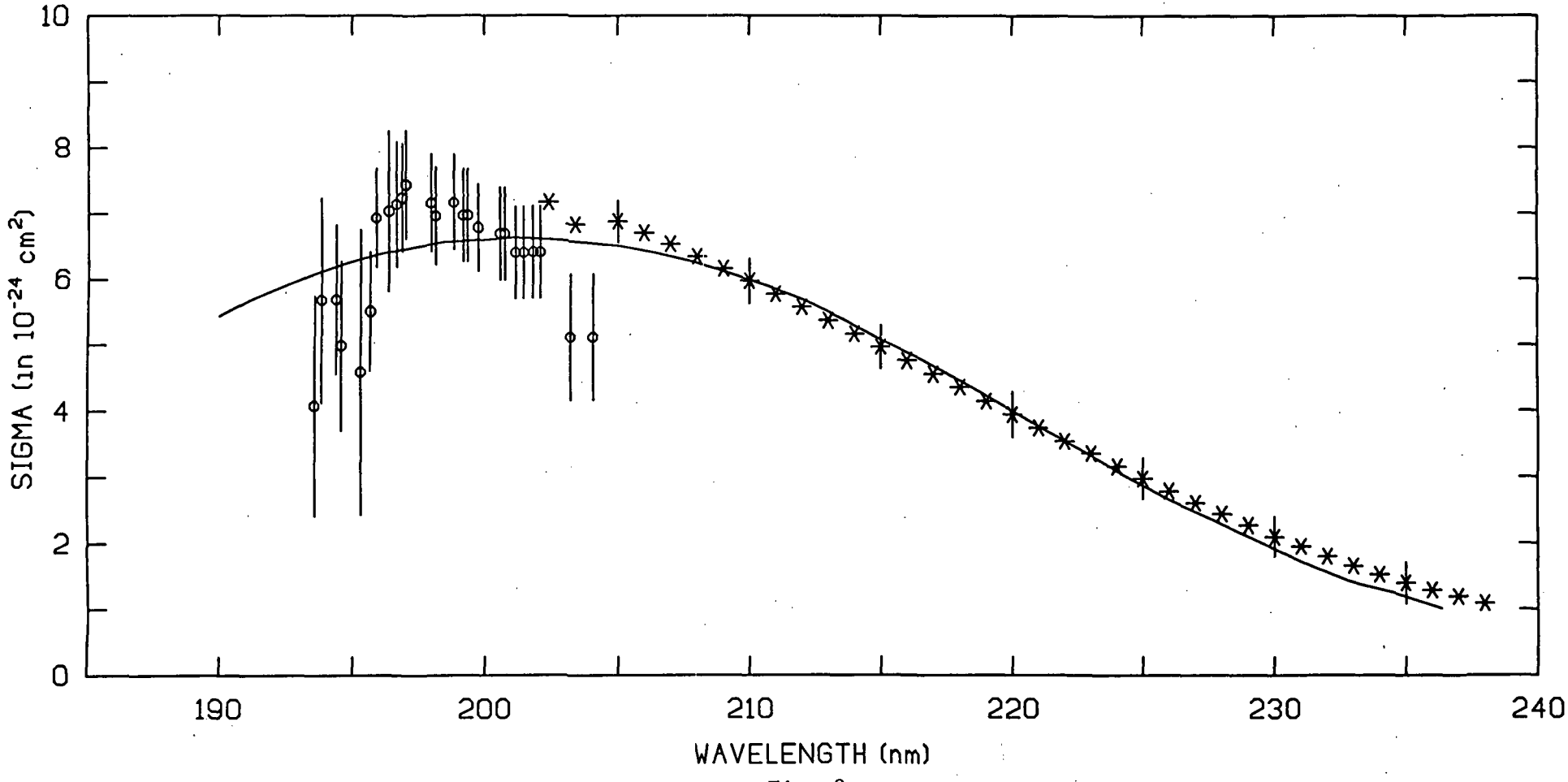
10
8
6
4
2
0
SIGMA (in 10^{-24} cm^2)
190
200
210
220
230
240
WAVELENGTH (nm)

Fig. 8